Supporting Information for:

Synthesis, Radical Reactivity and Thermochemistry of Monomeric Copper(II) Alkoxide Complexes Relevant to Copper/Radical Alcohol Oxidation Catalysis

*Thomas R. Porter, Dany Capitao, Werner Kaminsky, Zhaoshen Qian and James M. Mayer**

Department of Chemistry, University of Washington, Box 351700, Seattle, WA 98195-1700. Current address: Department of Chemistry, Yale University, 225 Prospect St., New Haven, CT 06520.

james.mayer@yale.edu

Contents:

1. Crystallographic Information

1.1 Crystallographic Information for $Tp^{tBu}Cu^{II}OCH_2CF_3$ (**1**)

An orange block, measuring 0.3 x 0.20 x 0.1 mm^3 was mounted on a glass capillary with oil. Data was collected at -163ºC on a Bruker APEX II single crystal X-ray diffractometer, Mo-radiation.

Crystal-to-detector distance was 40 mm and exposure time was 10 seconds per degree for all sets. The scan width was 0.5º. Data collection was 99.6% complete to 25º in ϑ. A total of 94153 (merged) reflections were collected covering the indices, h = -12 to 12, k = -22 to 22, l = -22 to 22. 13369 reflections were symmetry independent and the R_{int} = 0.0314 indicated that the data was good (average quality 0.07). Indexing and unit cell refinement indicated a primitive monoclinic lattice. The space group was found to be $P\ 2_1/n$ (No.14).

The data was integrated and scaled using SAINT, SADABS within the APEX2 software package by Bruker.

Solution by direct methods (SHELXS, SIR97) produced a complete heavy atom phasing model consistent with the proposed structure. The structure was completed by difference Fourier synthesis with SHELXL97. Scattering factors are from Waasmair and Kirfel.[1] Hydrogen atoms were placed in geometrically idealised positions and constrained to ride on their parent atoms with C---H distances in the range 0.95-1.00 Angstrom. Isotropic thermal parameters U_{eq} were fixed such that they were $1.2U_{eq}$ of their parent atom Ueq for CH's and $1.5U_{eq}$ of their parent atom U_{eq} in case of methyl groups. All non-hydrogen atoms were refined anisotropically by full-matrix least-squares.

[1] Waasmair, D.; Kirfel, A. *Acta Cryst. A.* **1995**, 51, 416.

Table S1: Crystallographic data for $Tp^{tBu}Cu^{II}OCH_2CF_3$ (**1**).

Empirical formula	$C_{23}H_{36}BCuF_3N_6O$	
Formula weight	543.93	
Temperature	110(2) K	
Wavelength	0.71073 Å	
Crystal system	Monoclinic	
Space group	P 2_1/n	
Unit cell dimensions	a = 9.6749(12) Å	α= 90°.
	b = 16.817(2) Å	β= 96.881(6)°.
	c = 16.646(2) Å	γ = 90°.
Volume	2688.9(6) Å^3	
Z	4	
Density (calculated)	1.344 Mg/m^3	
Absorption coefficient	0.860 mm^{-1}	
F(000)	1140	
Crystal size	0.30 x 0.30 x 0.10 mm^3	
Theta range for data collection	1.73 to 28.48°.	
Index ranges	-12<=h<=12, -22<=k<=22, -22<=l<=22	
Reflections collected	91453	
Independent reflections	6739 [R(int) = 0.0314]	
Completeness to theta = 25.00°	99.6 %	
Max. and min. transmission	0.9190 and 0.7825	
Refinement method	Full-matrix least-squares on F^2	
Data / restraints / parameters	6739 / 0 / 325	
Goodness-of-fit on F^2	1.036	
Final R indices [I>2sigma(I)]	R1 = 0.0276, wR2 = 0.0701	
R indices (all data)	R1 = 0.0343, wR2 = 0.0741	
Largest diff. peak and hole	0.661 and -0.292 e.Å^{-3}	

1.2 Crystallographic Information for $Tp^{tBuMe}Cu^{II}OCH_2CF_3$ (**2**).

An orange crystal, measuring 0.07 x 0.05 x 0.03 mm^3 and mounted on a loop with oil. Data was collected at -163ºC on a Bruker APEX II single crystal X-ray diffractometer, Mo-radiation.

Crystal-to-detector distance was 40 mm and exposure time was 20 seconds per frame for all sets. The scan width was 0.5º. Data collection was 99.9% complete to 25º in ϑ. A total of 68260 reflections were collected covering the indices, h = -11 to 11, k = -41 to 41, l = -11 to 11. 5391 reflections were symmetry independent and the R_{int} = 0.1214 indicated that the data was of slightly less than average quality (0.07). Indexing and unit cell refinement indicated a primitive monoclinic lattice. The space group was found to be $P\ 2_1/c$ (No.14).

The data was integrated and scaled using SAINT, SADABS within the APEX2 software package by Bruker.

Solution by direct methods (SHELXS, SIR97) produced a complete heavy atom phasing model consistent with the proposed structure. The structure was completed by difference Fourier synthesis with SHELXL97. Scattering factors are from Waasmair and Kirfel.[1] Hydrogen atoms were placed in geometrically idealised positions and constrained to ride on their parent atoms with C---H distances in the range 0.95-1.00 Angstrom. Isotropic thermal parameters U_{eq} were fixed such that they were $1.2U_{eq}$ of their parent atom Ueq for CH's and $1.5U_{eq}$ of their parent atom U_{eq} in case of methyl groups. All non-hydrogen atoms were refined anisotropically by full-matrix least-squares.

Table S2: Crystallographic data for $Tp^{tBuMe}Cu^{II}OCH_2CF_3$ (**2**).

Empirical formula	$C_{26}H_{42}BCuF_3N_6O$	
Formula weight	586.01	
Temperature	110(2) K	
Wavelength	0.71073 Å	
Crystal system	Monoclinic	
Space group	P 2_1/c	
Unit cell dimensions	a = 9.6817(16) Å	α= 90°.
	b = 34.735(6) Å	β= 115.495(10)°.
	c = 9.6425(16) Å	γ = 90°.
Volume	2926.9(8) Å^3	
Z	4	
Density (calculated)	1.330 Mg/m^3	
Absorption coefficient	0.795 mm^{-1}	
F(000)	1236	
Crystal size	0.07 x 0.05 x 0.03 mm^3	
Theta range for data collection	2.33 to 25.45°.	
Index ranges	-11<=h<=11, -41<=k<=41, -11<=l<=11	
Reflections collected	68260	
Independent reflections	5391 [R(int) = 0.1214]	
Completeness to theta = 25.00°	99.9 %	
Max. and min. transmission	0.9765 and 0.9465	
Refinement method	Full-matrix least-squares on F^2	
Data / restraints / parameters	5391 / 0 / 355	
Goodness-of-fit on F^2	1.008	
Final R indices [I>2sigma(I)]	R1 = 0.0435, wR2 = 0.0742	
R indices (all data)	R1 = 0.0804, wR2 = 0.0855	
Largest diff. peak and hole	0.377 and -0.403 e.Å^{-3}	

1.3.1 Crystallographic Information for $Tp^{tBuMe}Cu^{II}OCH(CH_3)CF_3$ (3)

An orange plate, measuring 0.21 x 0.20 x 0.17 mm^3 was mounted on a loop with oil. Data was collected at -163ºC on a Bruker APEX II single crystal X-ray diffractometer, Mo-radiation.

Crystal-to-detector distance was 40 mm and exposure time was 10 seconds per frame for all sets. The scan width was 0.5º. Data collection was 99.4% complete to 25º in ϑ. A total of 149335 reflections were collected covering the indices, h = -16 to 16, k = -32 to 31, l = -24 to 24. 13476 reflections were symmetry independent and the R_{int} = 0.0447 indicated that the data was of better than average quality (0.07). Indexing and unit cell refinement indicated a primitive monoclinic lattice. The space group was found to be $P\ 2_1/n$ (No.14).

The data was integrated and scaled using SAINT, SADABS within the APEX2 software package by Bruker.

Solution by direct methods (SHELXS, SIR97) produced a complete heavy atom phasing model consistent with the proposed structure. The structure was completed by difference Fourier synthesis with SHELXL97. Scattering factors are from Waasmair and Kirfel.[1] Hydrogen atoms were placed in geometrically idealised positions and constrained to ride on their parent atoms with C---H distances in the range 0.95-1.00 Angstrom. Isotropic thermal parameters U_{eq} were fixed such that they were $1.2U_{eq}$ of their parent atom Ueq for CH's and $1.5U_{eq}$ of their parent atom U_{eq} in case of methyl groups. All non-hydrogen atoms were refined anisotropically by full-matrix least-squares.

Extensive disorder of the $^{-}OCH(CH_3)CF_3$ ligand (over 4 different orientations) and of the pentane solvent caused the need of restraints on thermal parameters and distances of solvent and ligand to stabilize the refinement.

Table S3: Crystallographic data for $Tp^{tBu}Cu^{II}OCH(CH_3)CF_3$ (**3**).

Empirical formula	$C_{29}H_{50}BCuF_3N_6O$	
Formula weight	630.10	
Temperature	110(2) K	
Wavelength	0.71073 Å	
Crystal system	Monoclinic	
Space group	P 2_1/n	
Unit cell dimensions	a = 10.2492(13) Å	α= 90°.
	b = 20.261(3) Å	β= 90.045(6)°.
	c = 15.796(2) Å	γ = 90°.
Volume	3280.3(7) Å^3	
Z	4	
Density (calculated)	1.276 Mg/m^3	
Absorption coefficient	0.714 mm^{-1}	
F(000)	1340	
Crystal size	0.21 x 0.20 x 0.17 mm^3	
Theta range for data collection	1.63 to 34.22°.	
Index ranges	-16<=h<=16, -32<=k<=31, -24<=l<=24	
Reflections collected	149335	
Independent reflections	13476 [R(int) = 0.0447]	
Completeness to theta = 25.00°	99.4 %	
Max. and min. transmission	0.8882 and 0.8645	
Refinement method	Full-matrix least-squares on F^2	
Data / restraints / parameters	13476 / 322 / 530	
Goodness-of-fit on F^2	1.033	
Final R indices [I>2sigma(I)]	R1 = 0.0639, wR2 = 0.1514	
R indices (all data)	R1 = 0.0904, wR2 = 0.1725	
Largest diff. peak and hole	1.752 and -3.380 e.Å^{-3}	

1.3.2 X-Ray Crystal Structure of $Tp^{tBu}Cu^{II}OCH(CH_3)CF_3$ and Select Geometric Parameters.

The X-Ray Crystal Structure of $Tp^{tBu}Cu^{II}OCH(CH_3)CF_3$ has a solid state structure that is more tetrahedral than either (1) or (2) with a τ value of 0.63 (vs. 0.76 for both (1) and (2)).

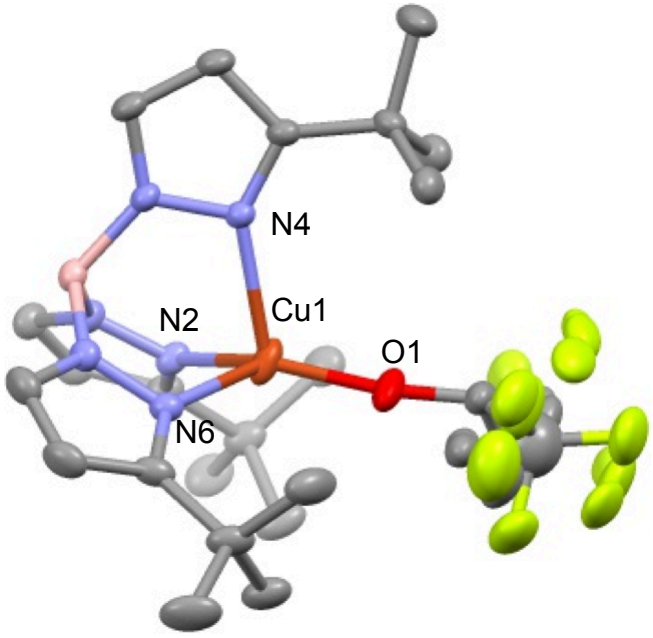

Figure S1. ORTEP drawing of $Tp^{tBu}Cu^{II}$-$OCH(CH_3)CF_3$. Hydrogen atoms are omitted for clarity. One pentane molecule co-crystallizes with $Tp^{tBu}Cu^{II}$-$OCH(CH_3)CF_3$ but is not shown here. The racemic $^{-}OC^{*}H(CH_3)CF_3$ ligand is disordered over 4 positions. Selected interatomic distances (Å) and angles (deg): N2-Cu1, 1.9733(16); N4-Cu1, 2.1740(15); N6-Cu1, 2.0640(16); Cu1-O1, 1.7923(17); O1-Cu1-N2, 137.53(8); O1-Cu-N6, 121.47(9); N2-Cu1-N6, 91.68(7); O1-Cu1-N4, 110.91(7); N2-Cu1-N4, 91.64(6); N6-Cu1-N4, 92.24(6). $\tau = 0.63$.

1.4 τ Value analysis of the X-ray structures of 1, 2, 3 and related structures.

The degree of geometric distortion from tetrahedral can be described quantitatively with the pyramidalization normalization parameter, τ, defined as:

$$\tau = [\Sigma (L_{basal}\text{-}M\text{-}L_{basal}) - \Sigma(L_{basal}\text{-}M\text{-}L_{axial})]/90$$

τ varies from 0 for a perfect tetrahedral to 1 for perfect trigonal monopyramidal.

Table S4. τ and EPR parameters for various $TpCu^{II}$-X complexes

Complex	τ value	EPR Signal	Ref.[a]
$Tp^{tBu}Cu^{II}OTf$	0.39	Rhombic	8a
$Tp^{tBuMe}Cu^{II}Cl$	0.44	NR[b]	9b
$Tp^{tBu}Cu^{II}Cl$	0.47	Rhombic	9a, 8d
$Tp^{tBu}Cu^{II}OCH(CH_3)CF_3$ **(3)**	0.63	Rhombic	This work
$Tp^{iPriPr}Cu^{II}SArF_5$[a]	0.64	Axial	10a
$Tp^{iPriPr}Cu^{II}OOCm$[a,b]	0.75	Axial	10b, 10f
$Tp^{tBu}Cu^{II}OCH_2CF_3$ (1)	0.76	Axial	This work
$Tp^{tBuMe}Cu^{II}OCH_2CF_3$ **(2)**	0.76	Axial	This work
$Tp^{iPriPr}Cu^{II}S^tBu$[a]	0.82	Axial	10c

[a] References refer to citations in the main text. [b] NR = not reported.
[c] Tp^{iPriPr} = hydro-t*ris*(3,5-di-*iso*-propyl-pyrazolyl)borate. [d] OOCm = cumyl peroxide.

2. Optical Spectra of 1, 2 and 3 in DCM.

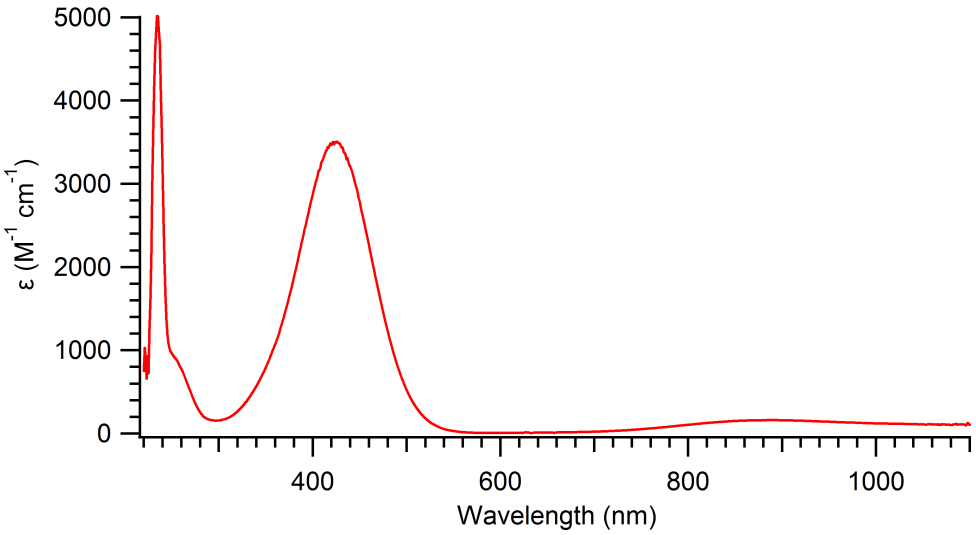

Figure S2. The Optical Spectrum of $Tp^{tBu}Cu^{II}OCH_2CF_3$ **(1)** in dichloromethane. λ_{max} = 424 nm (3500 ± 350 M^{-1} cm^{-1}), λ_{max} = 886 (160 ± 20 M^{-1} cm^{-1}).

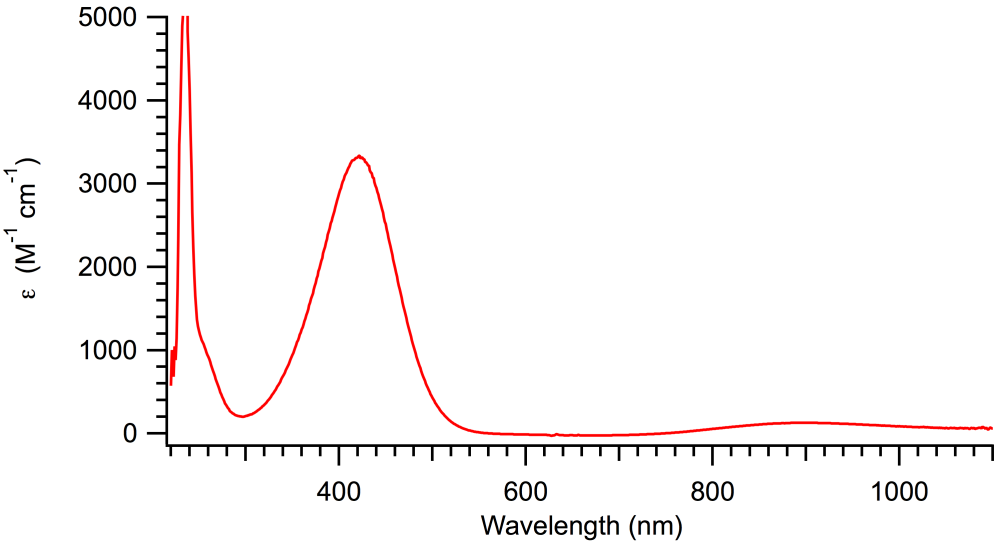

Figure S3. The Optical Spectrum of $Tp^{tBuMe}Cu^{II}OCH_2CF_3$ **(2)** in dichloromethane. λ_{max} = 423 nm (3300 ± 330 M^{-1} cm^{-1}), λ_{max} = 902 (130 ± 20 M^{-1} cm^{-1}).

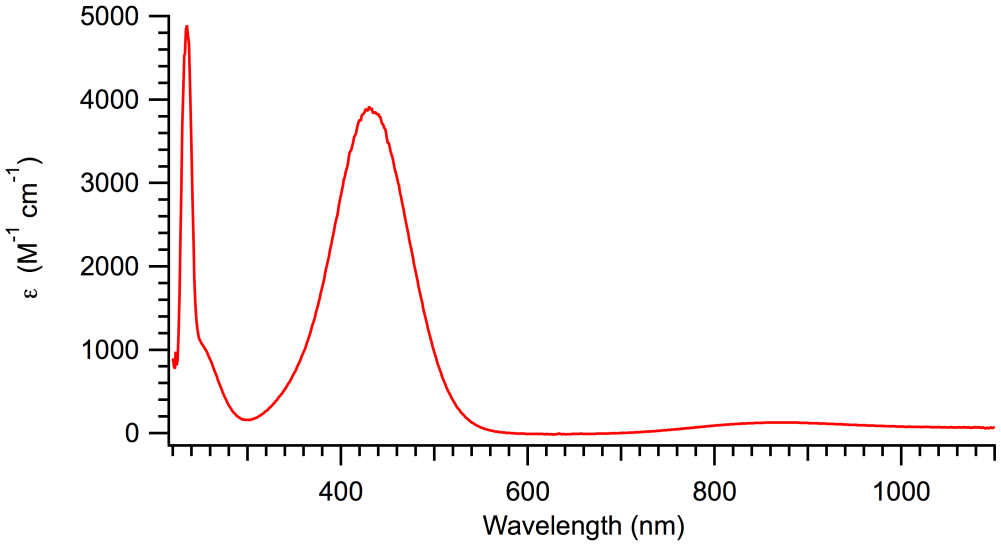

Figure S4. The Optical Spectrum of $Tp^{tBu}Cu^{II}$-$OCH(CH_3)CF_3$ **(3)** in dichloromethane. λ_{max} = 432 nm (3900 ± 390 M^{-1} cm^{-1}), λ_{max} = 869 (130 ± 20 M^{-1} cm^{-1}).

3. ^{1}H NMR Spectra of 2 and 3 in DCM-d_2.

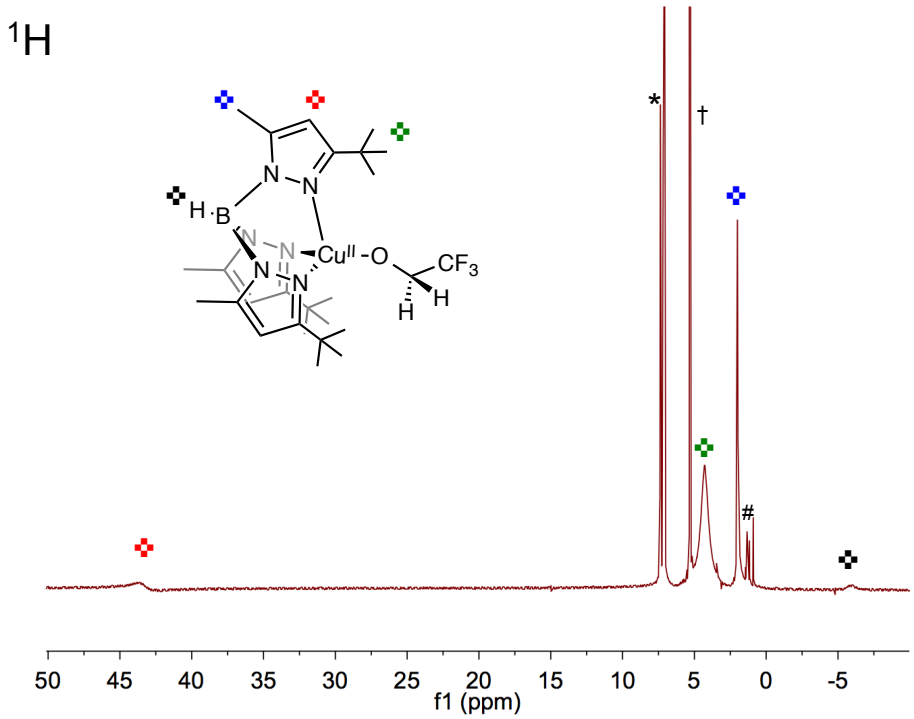

Figure S5. ^{1}H NMR spectrum of $Tp^{tBuMe}Cu^{II}OCH_2CF_3$ (**2**) in DCM-d_2. Peak assignments for **2** are shown by ✤. Residual solvent signal is annotated with † while a fluorobenzene internal standard is shown with *. The # symbol corresponds to trace diamagnetic impurities present.

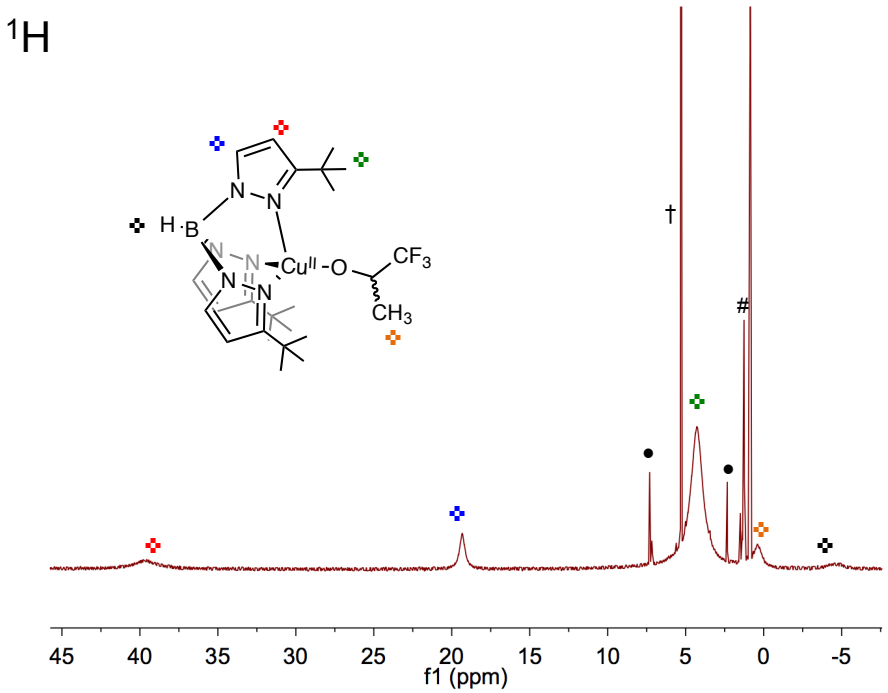

Figure S6. ^{1}H NMR spectrum of Tp^{tBu}Cu^{II}OCH(CH$_3$)CF$_3$ (**3**) in DCM-d_2. Peak assignments for **3** are shown by ✤. Residual solvent signal is annotated with †, residual toluene and ether from synthesis are shown with • and #, respectively.

Table S5. ^{1}H NMR Resonances of related Tp^{tBu}Cu^{II}-X and Tp^{tBuMe}Cu^{II}-X.[a,b]

Complex	*Pz-4-H*	*Pz-5-H*	*Pz-3-^{t}Bu*	B-H
Tp^{tBu}Cu^{II}Cl[§c,8a]	49.3	24.1	4.8	-4.4
Tp^{tBu}Cu^{II}OTf[§c,8a]	56.5	21.0	5.5	-5.4
1	40.5	18.4	4.4	-5.4
3	39.6	19.3	4.0	-4.6
	Pz-4-H	*Pz-5-CH$_3$*	*Pz-3-^{t}Bu*	B-H
Tp^{tBuMe}Cu^{II}Cl[§9b]	53.0	4.1	4.6	-5.1
Tp^{tBuMe}Cu^{II}OTf	59.0	10.4	4.5	-6.0
2	43.3	2.0	4.3	-5.9

[§]References refer to citations in the main text. [a] Values at 25° C. NMR spectra in dichloromethane-d_2, with chemical shifts in ppm; [b] NMR assignments for pz-4-H and pz-5-H were made by comparison to Tp^{tBuMe}Cu^{II} analogues. N.R. = not reported. [c] Complexes previously reported but without NMR characterization.

4. CW X-band EPR spectra and simulations of 1, 2 and 3.

Samples were prepared at concentrations of ~1.5 mM in toluene glasses. EPR spectra were collected on a Bruker EMX CW X-band spectrometer at 120 K. Data were simulated using the MATLAB 7.5 toolbox, EasySpin 4.5.5.[2] More complete analysis of the EPR spectra of **1** can be found in reference [3].

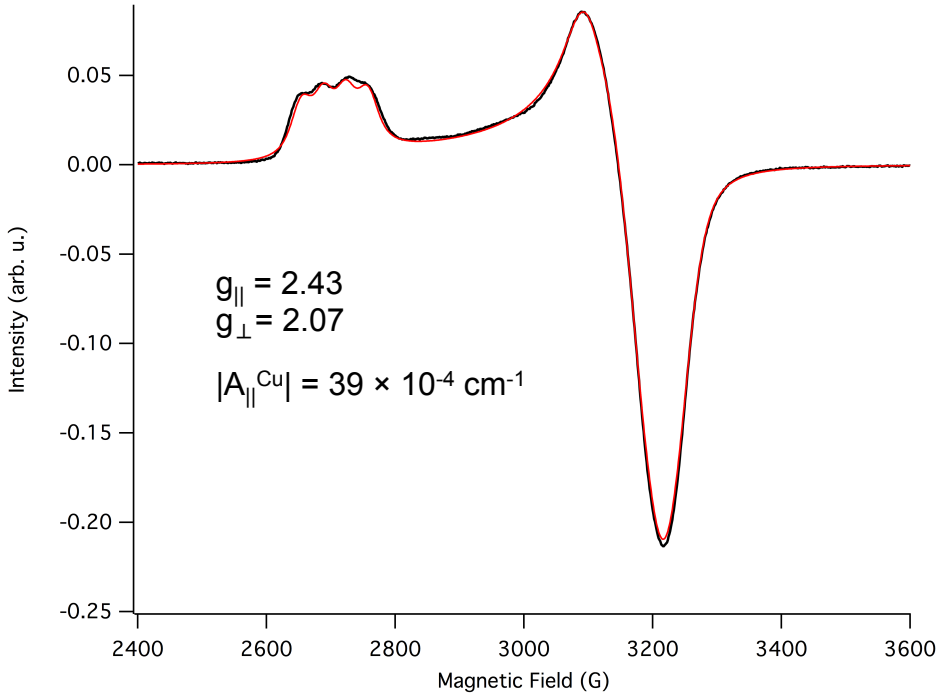

Figure S7. X-Band CW EPR Spectrum of 2.5 mM $Tp^{tBu}Cu^{II}OCH_2CF_3$ in a toluene glass at 120 K. Data is shown in black and simulation is shown in red.

[2] Stoll, S.; Schweiger, A. *J. Magn. Reson.* **2006**, 174, 42.

[3] Hayes, E. C.; Porter, T. R.; Barrows, C. J.; Kaminsky, W.; Mayer, J. M.; Stoll, S. *Submitted* Dec. 2015.

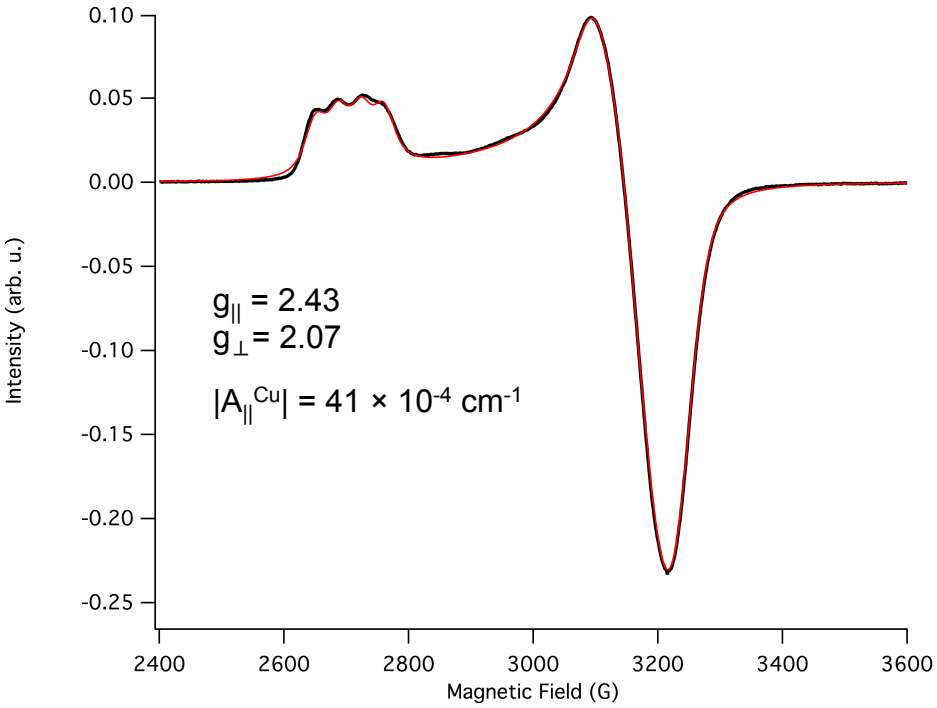

Figure S8. X-Band CW EPR Spectrum of 2.5 mM $Tp^{tBuMe}Cu^{II}OCH_2CF_3$ **(2)** in a toluene glass at 120 K. Data is shown in black and simulation is shown in red.

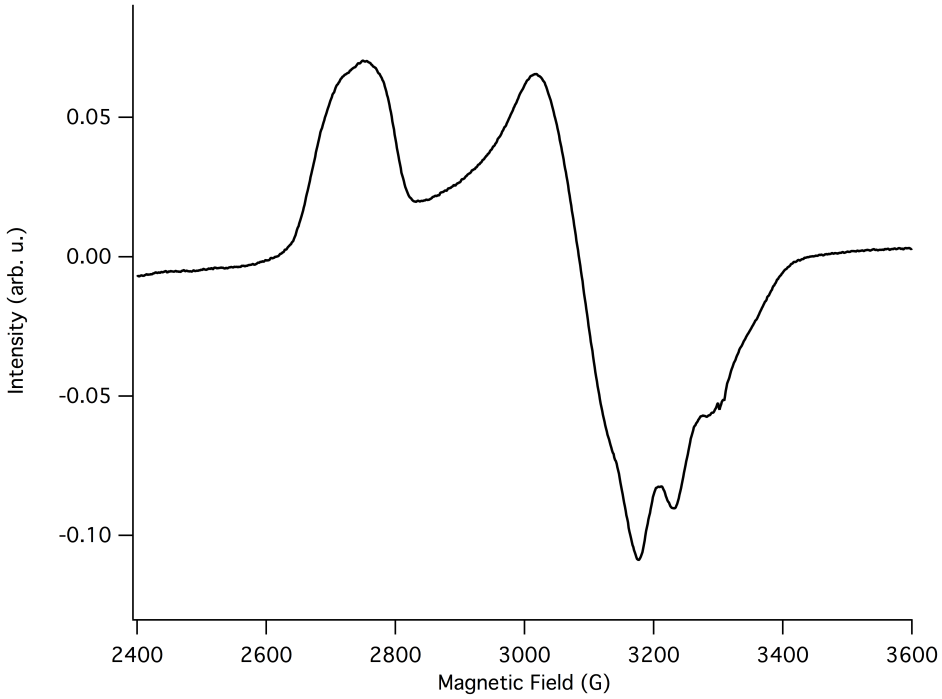

Figure S9. X-Band CW EPR Spectrum of 2.5 mM $Tp^{tBu}Cu^{II}OCH(CH_3)CF_3$ **(3)** in a toluene glass at 120 K (not simulated). The spectrum displays a rhombic signal unlike the axial signal observed for **1** or **2**.

5. Cyclic Voltammetry of 1, 2 and 3.

Cyclic voltammetry of **1**, **2** and **3** (~2.5 mM) was preformed in dichloromethane with 0.1 M [^{n}Bu$_4$N][PF$_6$] supporting electrolyte and a ferrocene internal standard. Scan rates used were 100 mV/s. Data was collected in a N_2 filled glovebox. The electrochemical setup consisted of a glassy carbon working electrode, silver *pseudo*-reference electrode and a platinum auxiliary electrode. Values reported are referenced to the ferrocene/ferrocenium couple.

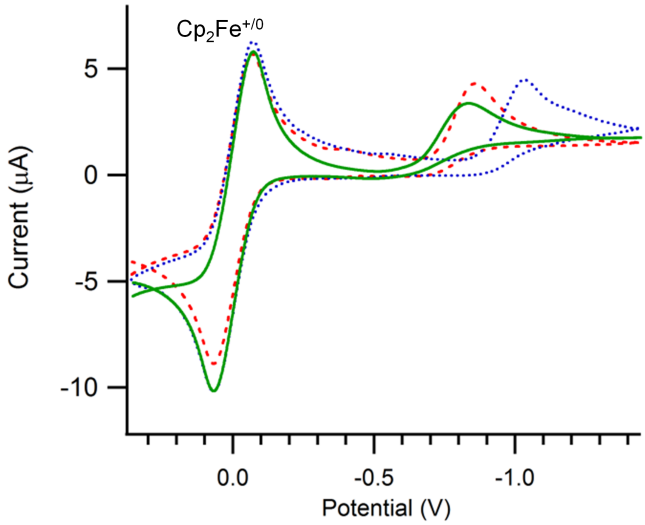

Figure S10. Cyclic voltammograms of 2.5 mM **1** (dashed red), **2** (dotted blue) and **3** (solid green) in dichloromethane at 100 mV s^{-1} under N_2 with 0.1 M [^{n}Bu$_4$N][PF$_6$] and a glassy carbon working electrode. The potential is referenced to the $Fc^{+/0}$ couple.

6. ^{1}H NMR spectra of 1 with one equivalent of [LutH$^+$][$^-$OTf].

$$Tp^{tBu}Cu^{II}OCH_2CF_3 + [LutH^+][^-OTf] + MeCN\text{-}d_3 \rightleftharpoons [Tp^{tBu}Cu^{II}(MeCN\text{-}d_3)^+][^-OTf] + HOCH_2CF_3$$

In a J. Young NMR tube, 15.3 mM $Tp^{tBu}Cu^{II}OCH_2CF_3$ in DCM-d_2/1% MeCN-d_3 (v/v) was combined with one equivalent of 2,6-lutidinium triflate. After ~ 20 minutes the ^{1}H NMR spectrum of the reaction solution was collected. Peak assignments for [$Tp^{tBu}Cu^{II}$(MeCN-d_3)$^+$][$^-$OTf] were confirmed by spiking a known sample of $Tp^{tBu}Cu^{II}$OTf with MeCN-d_3. In a separate control experiment, 2,6-lutidine was found to not displace MeCN-d_3 from [$Tp^{tBu}Cu^{II}$(MeCN-d_3^+)-[$^-$OTf] under these conditions.

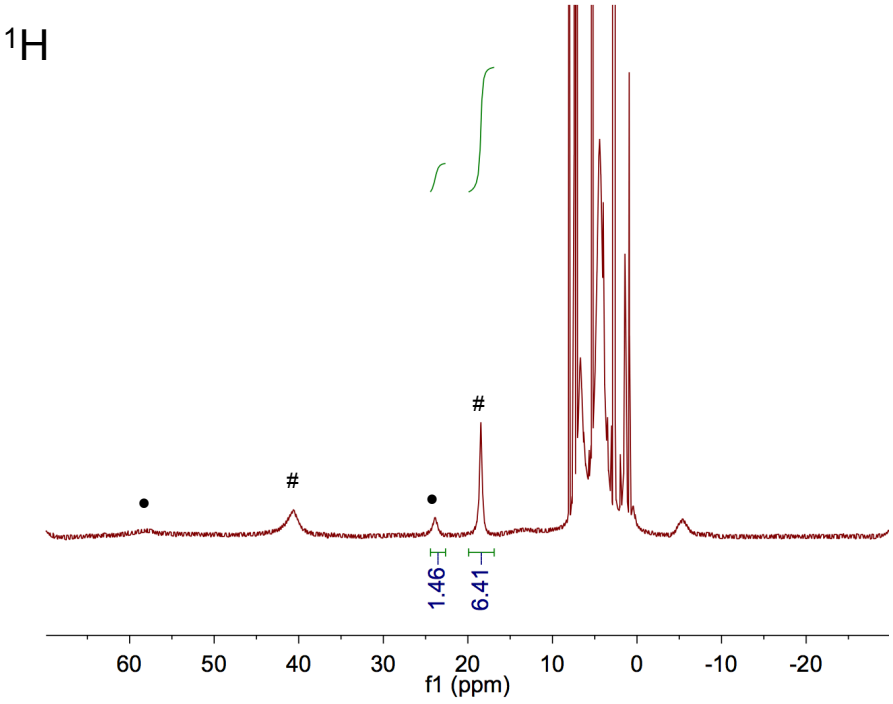

Figure S10. The ^{1}H NMR spectrum of the reaction between **2** and 2,6-lutidinium triflate in DCM-d_2/1% MeCN-d_3 (v/v). Complex **2** is shown with # and [$Tp^{tBu}Cu^{II}$(MeCN-d_3)$^+$] is shown with •. Relative integrations show a ~4:1 ratio of $Tp^{tBu}Cu^{II}OCH_2CF_3$/[$Tp^{tBu}Cu^{II}$(MeCN-d_3)$^+$].

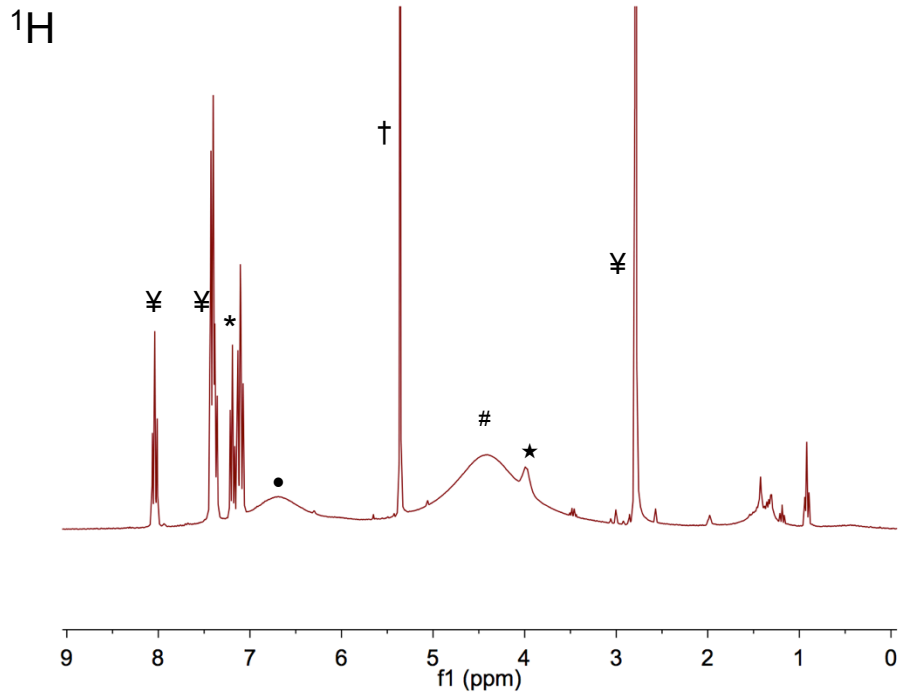

Figure S11. The expanded view of the ^{1}H NMR spectrum of the *pseudo*-equilibrium reaction between **2** and 2,6-lutidinium triflate in DCM-d_2/1% MeCN-d_3 (v/v). Complex **2** is shown with # and $[Tp^{tBu}Cu^{II}(MeCN\text{-}d_3)]^+$ is shown with •. 2,6-lutidinine/lutidinium triflate is shown with ¥, TFE with ★ and the residual solvent signal with †.

7. ^{1}H NMR Spectra of Tp^{tBu}Cu^{II}-OTf vs [Tp^{tBu}Cu^{II}-MeCN-$d_3$$^+$][OTf$^-$].

The ^{1}H NMR spectra of Tp^{tBu}Cu^{II}-OTf in DCM-d_2 or DCM-d_2 with 1% MeCN-d_3 (v/v) are dramatically different. We attribute this to the formation of [Tp^{tBu}Cu^{II}-MeCN$^+$][OTf$^-$] upon exposure of Tp^{tBu}Cu^{II}-OTf to MeCN-d_3.

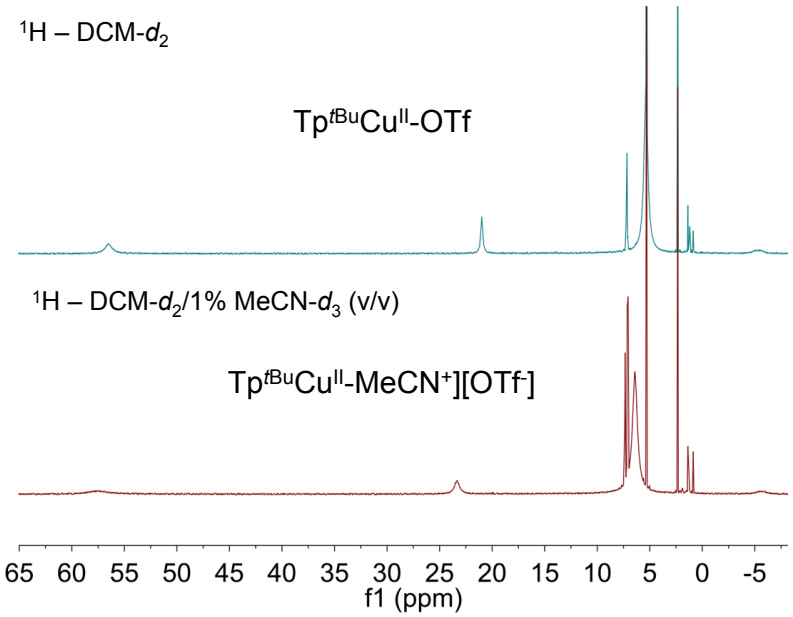

Figure S12. The ^{1}H NMR spectrum of Tp^{tBu}Cu^{II}-OTf in DCM-d_2 (top) and Tp^{tBu}Cu^{II}-MeCN$^+$][OTf$^-$] in DCM-d_2/1% MeCN-d_3 (v/v).

8. $[Tp^{tBu}Cu^{I}]_2$ in toluene-d_8 vs DCM-d_2/1% MeCN-d_3 (v/v).

In the absence of a Lewis base to occupy the vacant coordination site of copper in "$Tp^{tBu}Cu^{I}$", rapid formation and dissociation of $[Tp^{tBu}Cu]_2$ dimers[4] and adduct formation with trace solvent impurities complicate the ^{1}H NMR spectrum. This can be seen in the ^{1}H NMR spectrum of $[Tp^{tBu}Cu^{I}]_2$ in toluene. In DCM-d_2 with 1% MeCN-d_3 (v/v), MeCN-d_3 binds to the open coordination site forming 2 $Tp^{tBu}Cu^{I}$(MeCN-d_3) and the ^{1}H NMR is dramatically simplified.

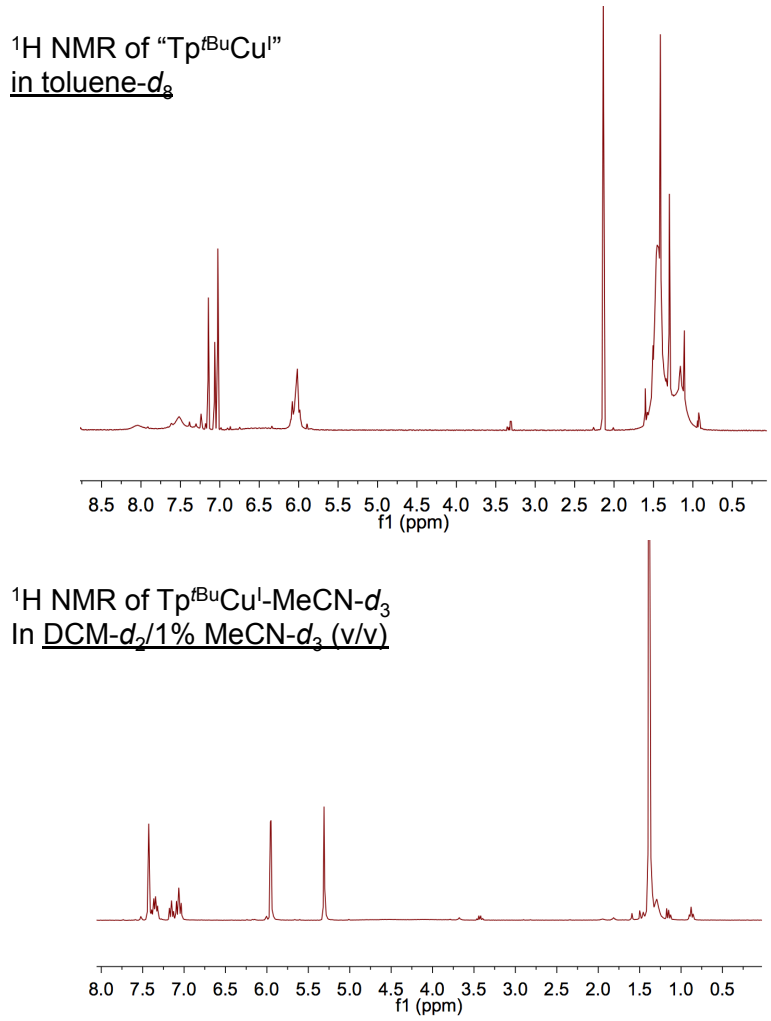

Figure S13. The ^{1}H NMR spectrum of "$Tp^{tBu}Cu^{I}$" in toluene-d_8 (top) and $Tp^{tBu}Cu^{I}$(MeCN-d_3) in DCM-d_2/1% MeCN-d_3 (v/v) with C_6H_5F internal standard (bottom).

(4) Carrier, S. M.; Ruggiero, C. E.; Houser, R. P.; Tolman, W. B. *Inorg. Chem.* **1993**, 32, 4889.

9. Attempts to prepare $Tp^{tBu}Cu^{II}$-OCH_2CH_3

In attempts to prepare a copper alkoxide with a non-fluorinated alkoxide ligand, a toluene-d_8 solution containing 15.3 mM $Tp^{tBu}Cu^{II}OTf$ was treated with 1.2 equivalents of ethanol and 1 equivalent of DBU. The ^1H NMR spectrum was collected within 10 minutes of mixing and displayed new paramagentically shifted peaks we have tentatively assigned to '$Tp^{tBu}Cu^{II}OCH_2CH_3$' as well as many unidentifiable diamagnetic side products. Attempts to isolate '$Tp^{tBu}Cu^{II}OCH_2CH_3$' were unsuccessful and led to further decomposition.

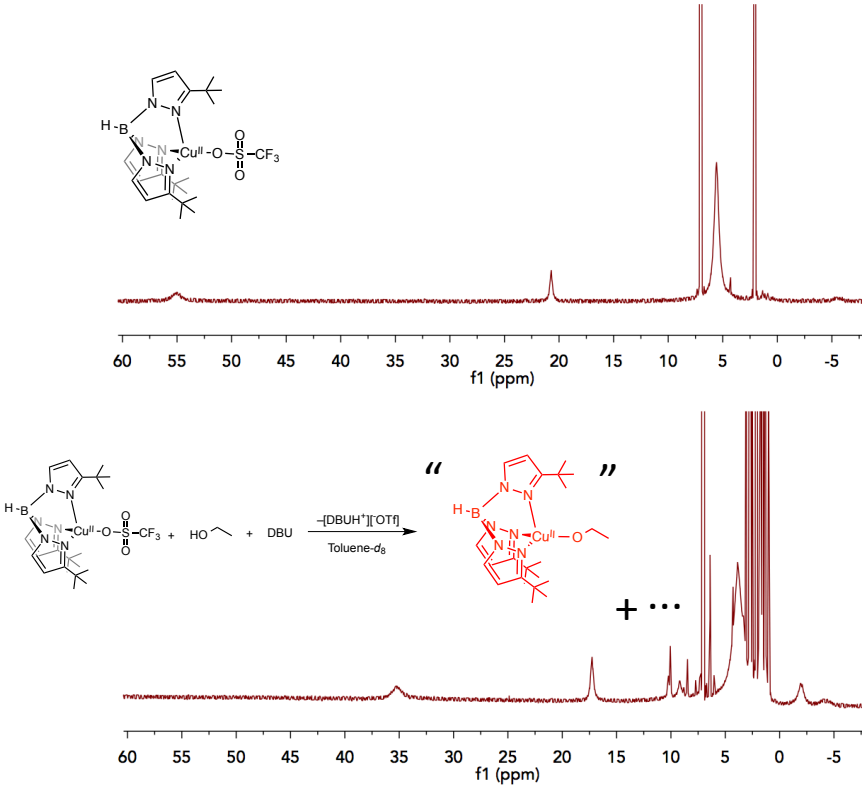

Figure S14. Stack of the ^1H NMR spectrum of $Tp^{tBu}Cu^{II}OTf$ (top) and the reaction between $Tp^{tBu}Cu^{II}$-OTf + 1.2 EtOH + DBU to generate "$Tp^{tBu}Cu^{II}OCH_2CH_3$ and various diamagnetic products (bottom); Both in toluene-d_8.

10. Select Reaction and Product Characterizations involving (1).

10.1. ^{1}H and ^{19}F NMR spectra of the completed reaction between 15.3 mM $Tp^{tBu}Cu^{II}OCH_2CF_3$ **(1)** and 1 eq TEMPO–H in DCM-d_2/1% MeCN-d_3 (v/v).

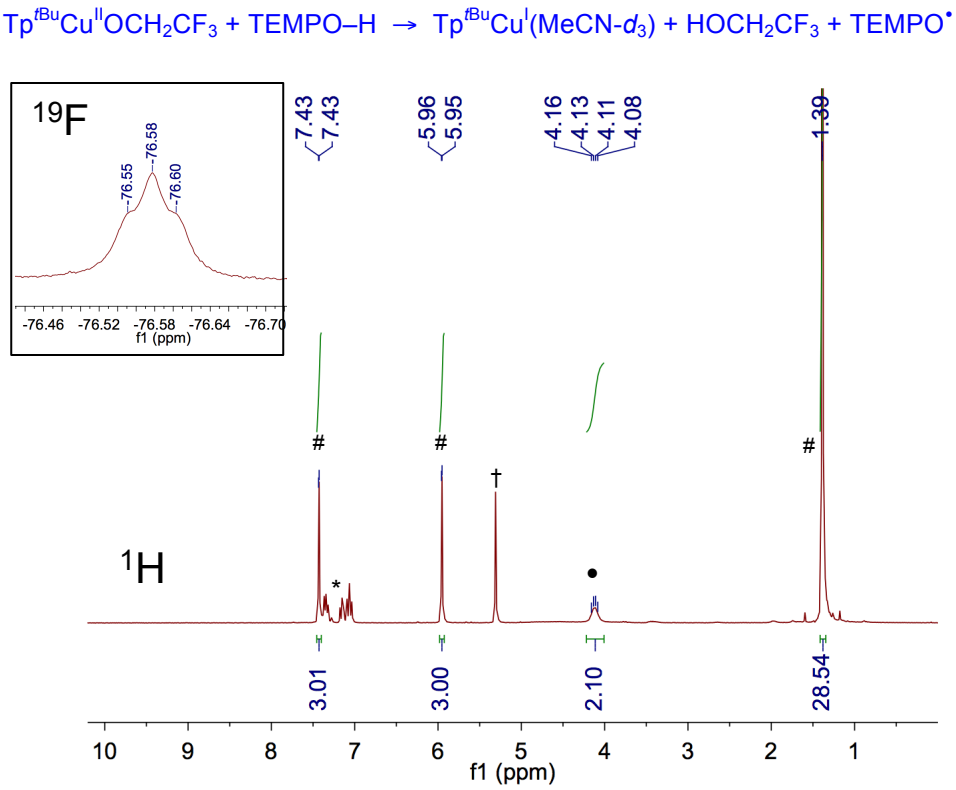

Figure S15. ^{1}H NMR spectrum of the completed reaction between 15.3 mM $Tp^{tBu}Cu^{II}OCH_2CF_3$ and 1 eq TEMPO–H in DCM-d_2/1% MeCN-d_3. Signals for $Tp^{tBu}Cu^{I}$-MeCN-d_3 are shown by # and 2,2,2-trifluoroethanol is shown by •. The fluorobenzene internal standard and residual solvent signals are labeled * and †, respectively. The ^{19}F NMR signal for 2,2,2-trifluoroethanol is shown in the inset.

10.2. Optical Spectrum of the completed reaction between 15.3 mM $Tp^{tBu}Cu^{II}OCH_2CF_3$ and $^tBu_3ArO–H$ in DCM-d_2/1% MeCN-d_3 (v/v).

The reaction between $Tp^{tBu}Cu^{II}$-OCH_2CF_3 and $^tBu_3ArO–H$ was carried out in an NMR tube with 15.3 mM $Tp^{tBu}Cu^{II}$-OCH_2CF_3 and one equivalent of $^tBu_3ArO–H$. After the reaction was complete (as determined by ^1H NMR) the solution was diluted with a stock solution of DCM/1%MeCN (v/v) to give an expected final concentration of products of 0.25 mM. The optical spectrum was collected and the absorption at 626 nm was found to be 0.102 absorbance units. This is consistent with the predicted final $^tBu_3ArO^\bullet$ concentration of 0.255 ± 0.020 as calculated from the reported exctincion coefficient ($\varepsilon_{626\ nm}$ = 400 ± 20 M^{-1} cm^{-1}).[5]

$$Tp^{tBu}Cu^{II}OCH_2CF_3 + {}^tBu_3ArO–H \rightarrow Tp^{tBu}Cu^{I}(MeCN\text{-}d_3) + HOCH_2CF_3 + {}^tBu_3ArO^\bullet$$

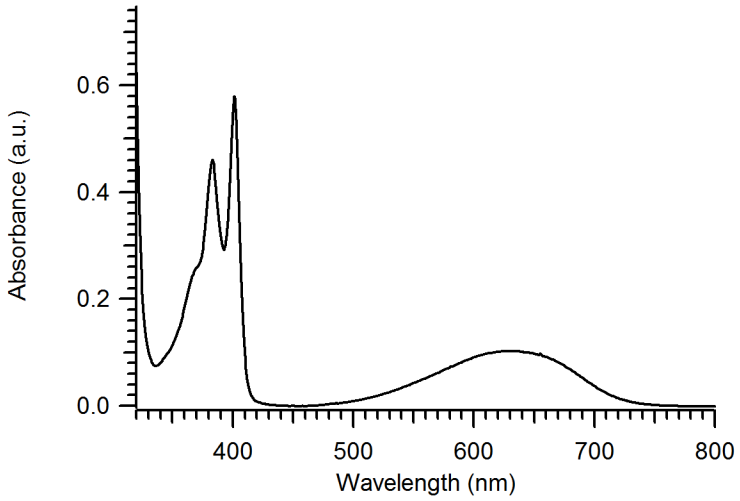

Figure S16. The UV/Vis spectrum of the completed reaction between $Tp^{tBu}Cu^{II}OCH_2CF_3$ and $^tBu_3ArO–H$ diluted for optical measurements.

(5) Manner, V. W.; Markle, T. F.; Freudenthal, J. H.; Roth, J. P.; Mayer, J. M. *Chem. Commun.* **2008**, 256.

10.3. The ^{1}H NMR spectrum of the completed reaction between 15.3 mM Tp^{tBu}Cu^{II}OCH$_2$CF$_3$ and 50 equivalents 1,4-cyclohexadiene in DCM-d_2/1% MeCN-d_3 (v/v).

The reaction between Tp^{tBu}Cu^{II}OCH$_2$CF$_3$ and 1,4-cyclohexadiene (1,4-CHD) requires 2 weeks to reach completion. The reaction was carried out in a J. Young NMR tube covered with aluminum foil and stored in a nitrogen filled glovebox. The benzene generated roughly equated to 0.5 equivalents with respect to initial Tp^{tBu}Cu^{II}OCH$_2$CF$_3$ after correcting for the benzene impurity previously present in 1,4-cyclohexadiene and the overlapping reference peaks (fluorobenzene).

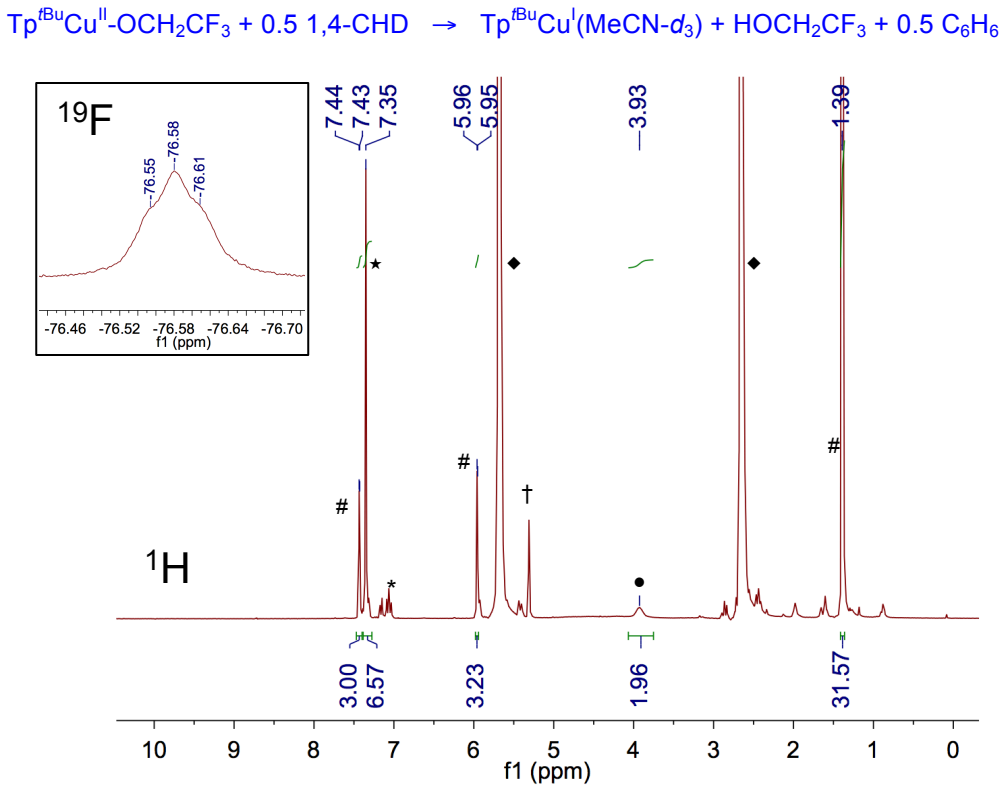

Figure S17. ^{1}H NMR spectrum of the completed reaction between 15.3 mM Tp^{tBu}Cu^{II}OCH$_2$CF$_3$ and 50 eq 1,4-cyclohexadiene in DCM-d_2/1% MeCN-d_3. Signals for Tp^{tBu}Cu^{I}(MeCN-d_3) are shown with #, 2,2,2-trifluoroethanol is shown with •.and benzene is shown with ★. The fluorobenzene internal standard and residual solvent signals are labeled * and †, respectively. The remaining 1,4-cyclohexadiene is shown with ◆. The ^{19}F NMR signal for 2,2,2-trifluoroethanol is shown in the inset.

10.4. ^{1}H NMR and Optical Spectrum for the Completed Reaction Between 15.3 mM $Tp^{tBu}Cu^{II}OCH_2CF_3$ and one equivalent of 2,6-^{t}Bu$_2$-4-(4-nitrophenyl)phenol [^{t}Bu$_2$(O$_2$NC$_6$H$_4$)C$_6$H$_2$O–H].

An NMR tube was charged with 15.3 mM $Tp^{tBu}Cu^{II}OCH_2CF_3$ and one equivalent of 2,6-^{t}Bu$_2$-4-(4-nitrophenyl)phenol in DCM-d_2/1% MeCN-d_3 (v/v). After the reaction was complete (as determined by ^{1}H NMR) the solution was diluted with a stock solution of DCM/1%MeCN (v/v) to give an expected final concentration of products of 2.0 mM. The optical spectrum was collected and the absorption at 625 nm was found to be 1.02 absorbance units, corresponding to a final 2,6-^{t}Bu$_2$-4-(4-nitrophenyl)phenoxyl concentration of 1.96 ± 0.20 mM as calculated from the reported exctincion coefficient ($\varepsilon_{626\ nm}$ = 520 ± 25 M^{-1} cm^{-1}).[6] This is consistent with the predicted concentration of 2.0 mM.

$Tp^{tBu}Cu^{II}$-OCH_2CF_3 + ^{t}Bu$_2$(O$_2$NC$_6$H$_4$)C$_6$H$_2$O–H → $Tp^{tBu}Cu^{I}$(MeCN-d_3) + $HOCH_2CF_3$ + ^{t}Bu$_2$(O$_2$NC$_6$H$_4$)C$_6$H$_2$O$^\bullet$

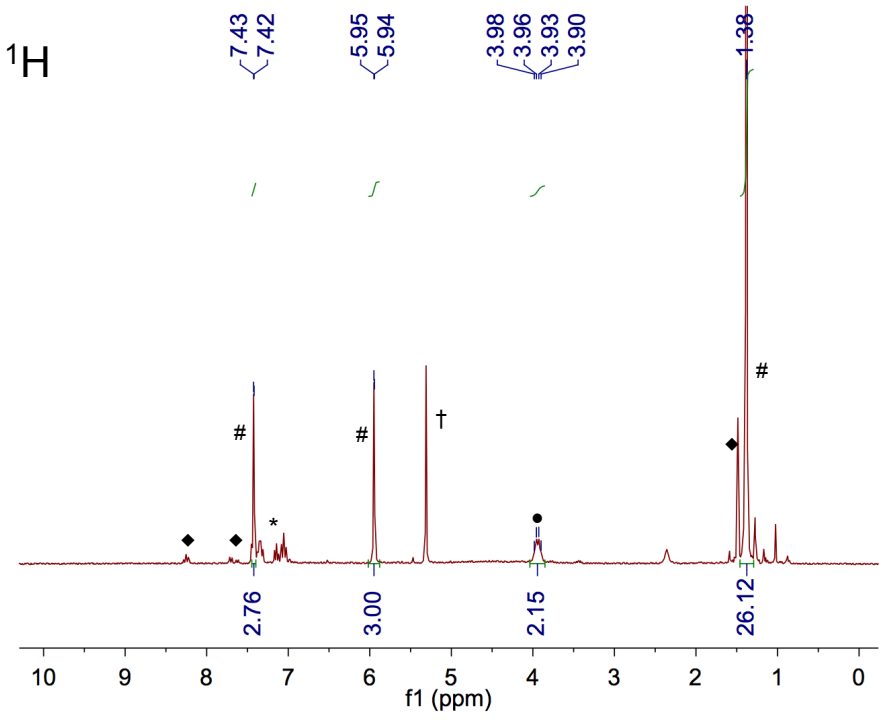

Figure S18. ^{1}H NMR spectrum of the completed reaction between 15.3 mM $Tp^{tBu}Cu^{II}OCH_2CF_3$ and 1 equivalent 2,6-^{t}Bu$_2$-4-(4-nitrophenyl)phenol in DCM-d_2/1% MeCN-d_3. Signals for $Tp^{tBu}Cu^{I}$-MeCN-d_3 are shown with #, 2,2,2-trifluoroethanol is shown with •. Trace excess ^{t}Bu$_2$NPArO–H is show with ◆, residual solvent signal with † and the fluorobenzene internal standard with *.

(6) Porter, T. R.; Kaminsky, W.; Mayer, J. M. *J. Org. Chem.* **2014**, 79, 9451.

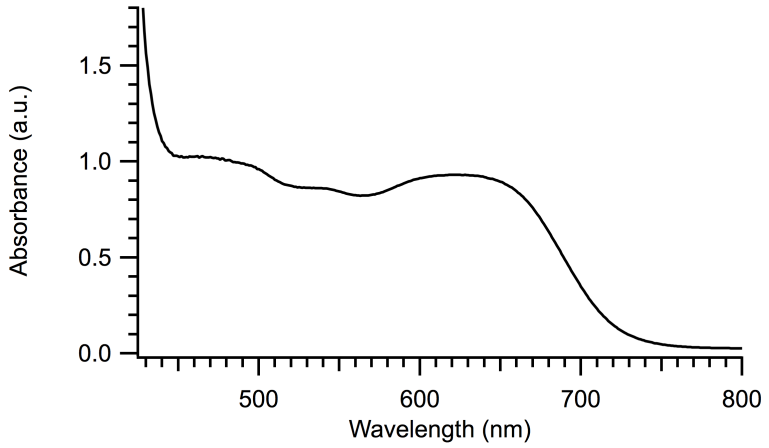

Figure S19. The UV/Vis spectrum of the completed reaction between $Tp^{tBu}Cu^{II}OCH_2CF_3$ and 1 equivalent 2,6-^{t}Bu$_2$-4-(4-nitrophenyl)phenol in DCM-d_2/1% MeCN-d_3, diluted to 2 mM for optical measurements.

10.5. NMR Spectra of the Completed Disproportionation Reaction of 15.3 mM $Tp^{tBu}Cu^{II}OCH_2CF_3$ catalyzed with 1 eq TEMPO in DCM-d_2/1% MeCN-d_3 (v/v).

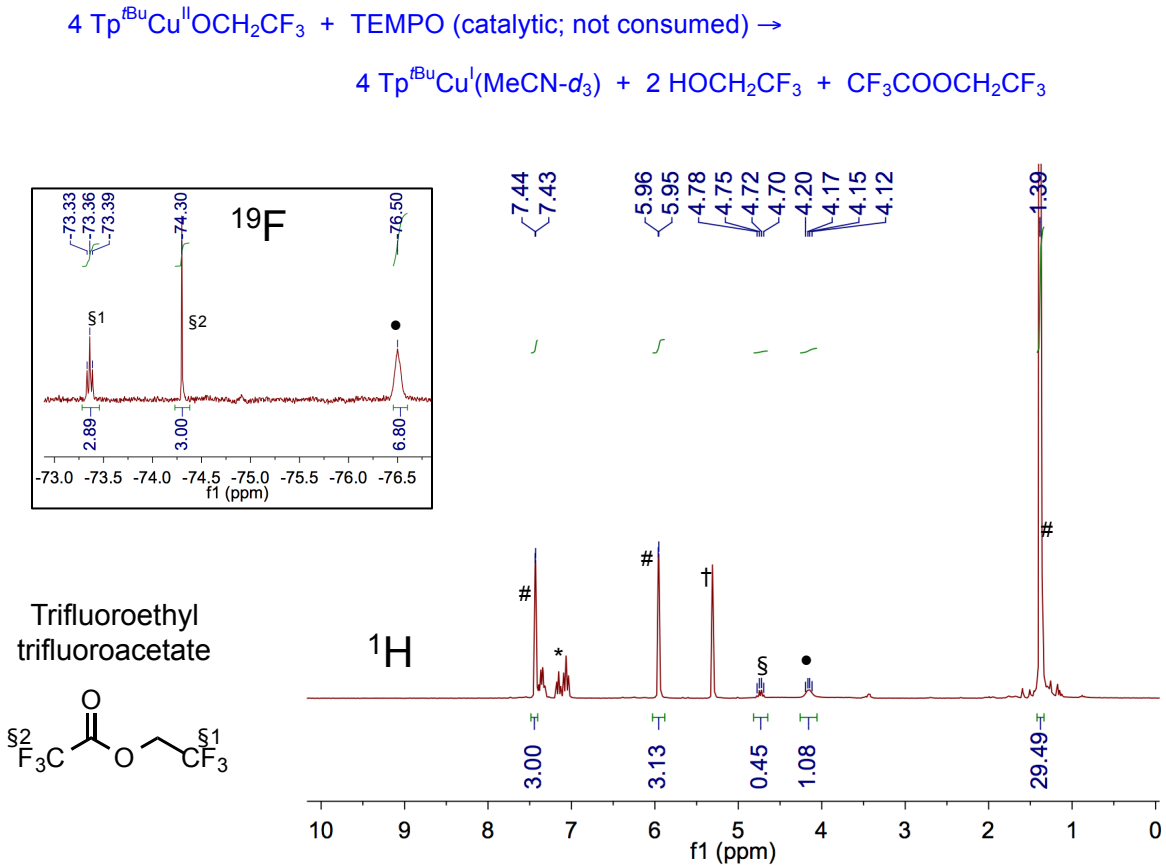

Figure S20. The ^{1}H NMR spectrum of the completed reaction between $Tp^{tBu}Cu^{II}OCH_2CF_3$ and catalytic TEMPO showing the production of $Tp^{tBu}Cu^{I}$(MeCN-d_3) (#), 0.5 eq 2,2,2-trifluoroethanol (•) and 0.25 eq trifluoroethyl trifluoroacetate (§). The residual solvent signals is shown with † and the fluorobenzene internal standard is shown with *. Inset displays the ^{19}F NMR spectrum of the same reaction mixture.

10.6. Kinetic Trace for the Disproportionation Reaction of 15.3 mM $Tp^{tBu}Cu^{II}OCH_2CF_3$ catalyzed with 1 eq TEMPO in DCM-d_2/1% MeCN-d_3 (v/v)

$$4\ Tp^{tBu}Cu^{II}\text{-}OCH_2CF_3\ +\ \text{TEMPO (catalytic; not consumed)} \rightarrow$$
$$4\ Tp^{tBu}Cu^{I}(MeCN\text{-}d_3)\ +\ 2\ HOCH_2CF_3 +\ CF_3COOCH_2CF_3$$

The kinetic trace for this reaction was obtained by preparing a 15.3 mM DCM-d_2/1%MeCN-d_3 (v/v) solution of $Tp^{tBu}Cu^{II}OCH_2CF_3$ and one eq TEMPO in a J. Young NMR tube in a nitrogen filled glovebox. Shortly after mixing (*ca*. 5 minutes), ^{1}H NMR spectra were collected at 5 minute intervals until the reaction had reached completion. Only 1 scan per spectrum was collected in order to ensure complete T1 relaxation was reached between scans. Reaction progress was monitored by integration of the $Tp^{tBu}Cu^{I}(MeCN\text{-}d_3)$ pyrazole peak at δ 5.95 ppm vs. a fluorobenzene internal standard (shown below with ∘). The same experiment was performed with the $Tp^{tBu}Cu^{II}OCD_2CF_3$ isotopologue (shown below with ×).

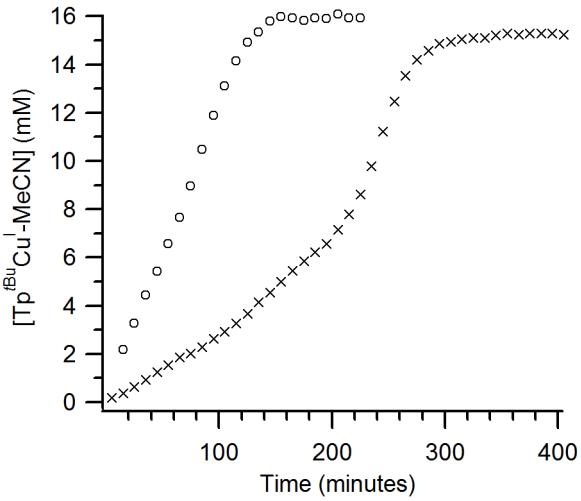

Figure S21. Kinetic traces for the disproportionation reaction of $Tp^{tBu}Cu^{II}OC(H/D)_2CF_3$ catalyzed by 1 eq TEMPO. The trace for $Tp^{tBu}Cu^{II}OCH_2CF_3$ is shown with ∘ while the trace for $Tp^{tBu}Cu^{II}OCD_2CF_3$ is shown with ×.

10.7. NMR spectra of the completed reaction between 15.3 mM Tp^{tBu}Cu^{II}OCH$_2$CF$_3$ and ^{t}Bu$_3$ArO$^\bullet$ in DCM-d_2/1% MeCN-d_3 (v/v) and characterization of ^{t}Bu$_3$CHDO-TFE.

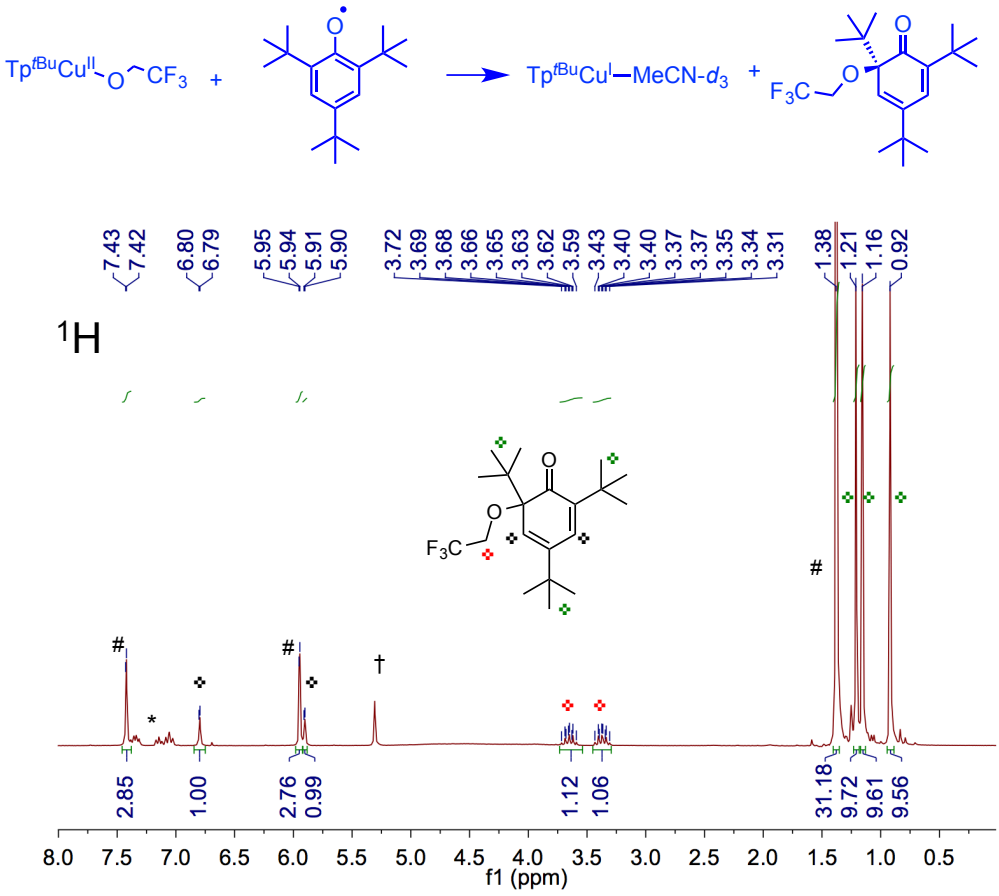

Figure S22. ^{1}H NMR spectrum of the completed reaction between 15.3 mM Tp^{tBu}Cu^{II}-OCH$_2$CF$_3$ and 1 eq ^{t}Bu$_3$ArO$^\bullet$ in DCM-d_2/1% MeCN-d_3 (v/v). Signals for Tp^{tBu}Cu^{I}–MeCN-d_3 are shown with # and signals for ^{t}Bu$_3$CHDO-TFE are shown with ✤. The fluorobenzene internal standard is shown with *.

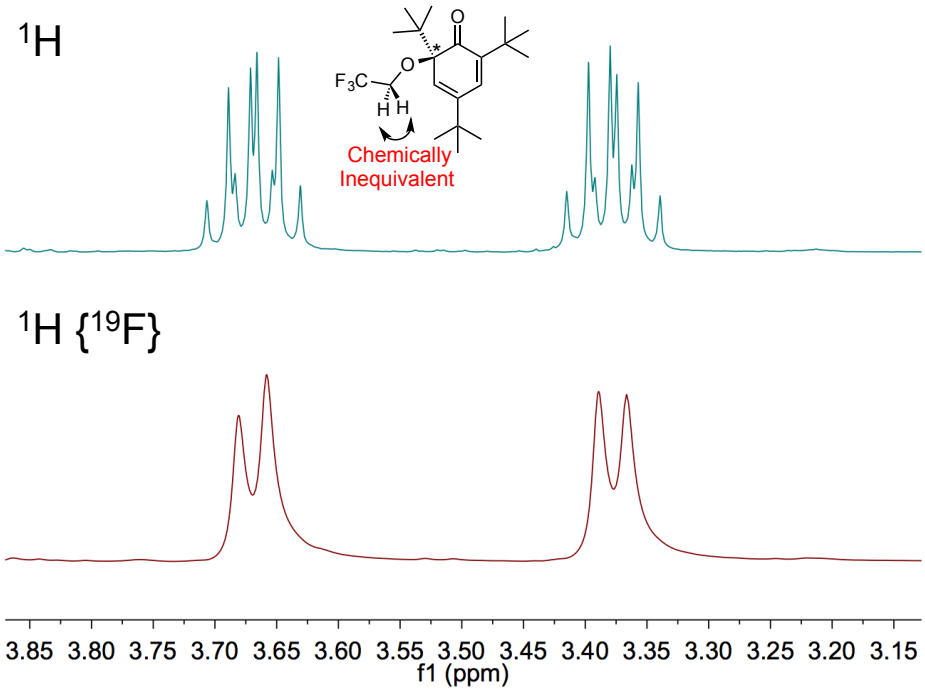

Figure S23. Expanded view of the ^{1}H (top) and ^{1}H {^{19}F} (bottom) NMR spectra (500 MHz, in DCM-d_2/1% MeCN-d_3 (v/v)) of ^{t}Bu$_3$CHDO-TFE, **4**, displaying the signals for the trifluoroethyl ether methylene -CH$_2$ unit.

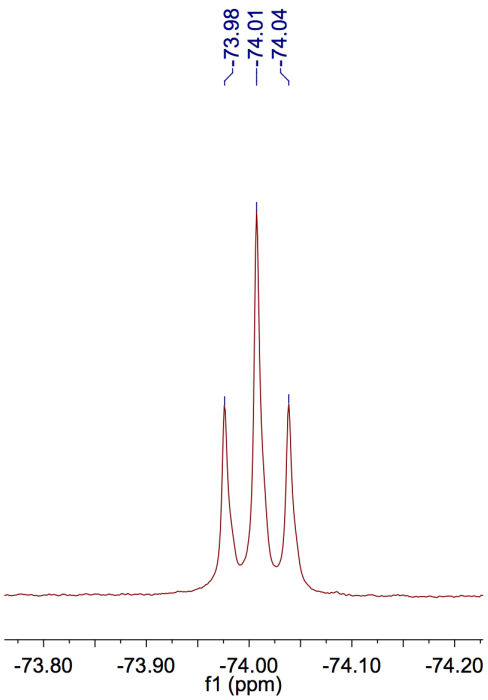

Figure S24. ^{19}F NMR spectrum of ^{t}Bu$_3$CHDO-TFE (282 MHz, in DCM-d_2/1% MeCN-d_3 (v/v)).

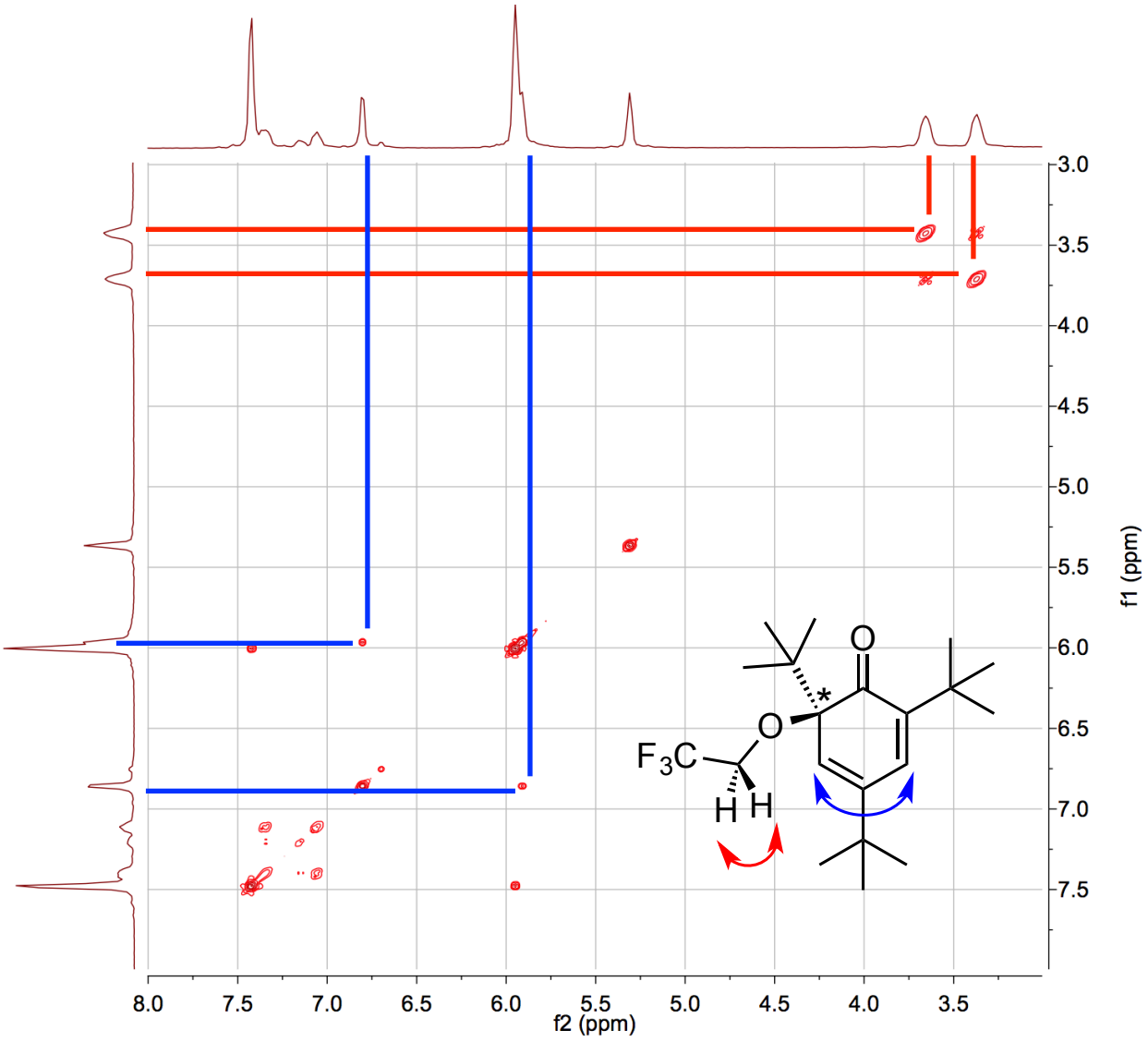

Figure S25. COSY spectrum of the completed reaction between 15.3 mM $Tp^{tBu}Cu^{II}OCH_2CF_3$ and 1 equivalent of $^tBu_3ArO^\bullet$ in DCM-d_2/1% MeCN-d_3.

From these NMR experiments, the following assignments were made: ^{1}H NMR of $^tBu_3$CHDO-TFE (300 MHz, DCM-d_2, 1% MeCN-d_3 (v/v), fluorobenzene int. std.): δ 6.80 (d, $^4J_{HH}$ = 2.4 Hz, 1H), 5.91 (d, $^4J_{HH}$ = 2.4 Hz, 1H), 3.66 (dq, $^2J_{HH}$ = 11.4 Hz, $^3J_{HF}$ = 9.0 Hz, 1H), 3.37 (dq, $^2J_{HH}$ = 11.4 Hz, $^3J_{HF}$ = 9.0Hz), 1.22 (s, 9H), 1.16 (s, 9H), 0.93 (s, 9H). ^{19}F NMR (282 MHz, DCM-d_2, 1% MeCN-d_3 (v/v), fluorobenzene int. std.): δ −73.95 (t, $^3J_{HF}$ = 9.0 Hz, 3F).

10.8. GC/MS of $^{t}Bu_3$CHDO-TFE

We found isolation of $^{t}Bu_3$CHDO-TFE difficult because of the small scales in which it was produced. However, GC/MS (electron impact ionization) of the crude reaction material displays a chromatogram with a large peak displaying an M^+ signal at 304 m/z that we have assigned to $^{t}Bu_3$CHDO-TFE minus isobutylene. This seems like a reasonable assignment considering hard ionization source used.

10.9. IR Spectroscopy of the completed reaction mixture containing $Tp^{tBu}Cu^{I}$-MeCN-d_3 and $^{t}Bu_3$CHDO-TFE.

Similarly, because isolation of $^{t}Bu_3$CHDO-TFE was problematic, the IR spectrum of the entire reaction mixture was collected (NaCl plate). The peak observed at 1670 cm^{-1} was assigned to the C=O stretch of $^{t}Bu_3$CHDO-TFE. This stretch is in good agreement with related quinoidal species which have values in the same range (1670 – 1700 cm^{-1}). [7]

(7) Pelter, A.; Elgendy, S. M. A. *J. Chem. Soc. Perkin Trans. 1* **1993**, 1891.

10.10. Pseudo-First Order Kinetic Measurements for $Tp^{tBu}Cu^{II}OCH_2CF_3$ plus $^tBu_3ArO^\bullet$ in DCM/1% MeCN (v/v).

In each measurement, a cuvette equipped with a gas tight septum was filled with a known concentration of $^tBu_3ArO^\bullet$ (8.9 – 88.6 mM) in DCM/MeCN 1% (v/v). $Tp^{tBu}Cu^{II}OCH_2CF_3$ was injected into the cuvette from a gastight syringe (to give a final concentration of 0.5 mM) immediately prior to starting kinetic measurements. The kinetics were monitored by UV/Vis spectroscopy. The large excess of $^tBu_3ArO^\bullet$ saturated most of the signal from $Tp^{tBu}Cu^{II}OCH_2CF_3$ but monitoring the optical change between 400 and 500 nm proved sufficient for tracking reaction progress. Data were fit by SPECFIT/32™ global analysis program to a simple first order model. The second order rates calculated were generally reproducible when the same solvent batch was used for measurements but were irreproducible between stock solvents or even when the same stock solvent was used on different days.

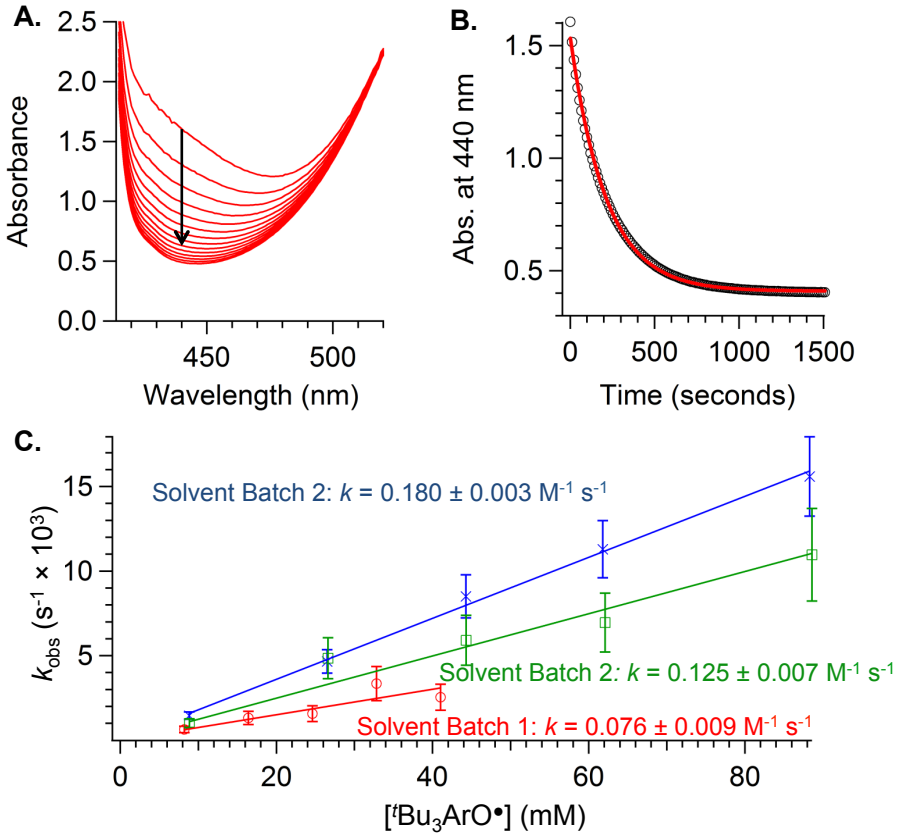

Figure S26. (A) Selected optical spectra of the reaction between $Tp^{tBu}Cu^{II}OCH_2CF_3$ (0.5 mM) with $^tBu_3ArO$ (26.5 mM). (B) Kinetic trace of the same reaction monitored at 440 nm. The raw data is indicated by black circles (∘) and the solid red line represents the single exponential fit. (C) The pseudo-first order plot of the reaction between $Tp^{tBu}Cu^{II}OCH_2CF_3$ and $^tBu_3ArO$ collected with three different solvent batches under similar conditions.

10.11. Kinetic Traces of $Tp^{tBu}Cu^{II}$-OCH_2CF_3 and $Tp^{tBu}Cu^{II}$-OCD_2CF_3 with 1 eq $^tBu_3ArO^\bullet$ Using the Same Batch of Solvent (DCM-d_2/1% MeCN-d_3 (v/v).

The kinetic trace for these reactions was obtained by preparing a 15.3 mM DCM-d_2/1%MeCN-d_3 (v/v) solution of either $Tp^{tBu}Cu^{II}$-OCH_2CF_3 or $Tp^{tBu}Cu^{II}$-OCD_2CF_3 with one eq TEMPO in a J. Young NMR tube in a nitrogen filled glovebox. Shortly after mixing (*ca*. 5 minutes), ^{1}H NMR spectra were collected at 5 minute intervals until the reaction had reached completion. Only 1 scan per spectrum was collected in order to ensure complete T1 relaxation was reached between scans. Reaction progress was monitored by integration of the $Tp^{tBu}Cu^{I}$-MeCN-d_3 pyrazole peak at δ 5.95 ppm vs. a fluorobenzene internal standard. The same experiment was performed with the $Tp^{tBu}Cu^{II}$-OCD_2CF_3 isotopologue and is also shown. Within the error of the experiment (± ~10 %), no kinetic isotope effect is observed.

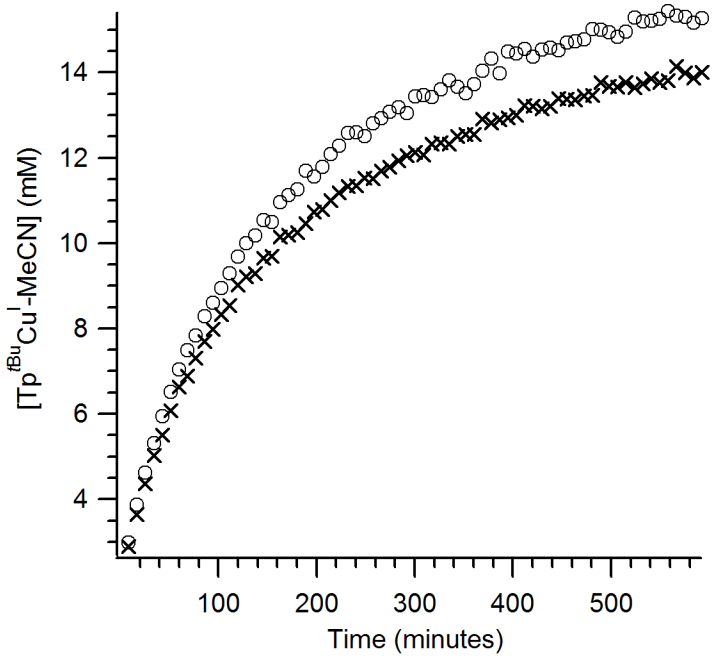

Figure S27. Kinetic Trace for the Reactions of 15.3 mM $Tp^{tBu}Cu^{II}$-OCH_2CF_3 (∘) and $Tp^{tBu}Cu^{II}$-OCD_2CF_3 (×) with 1 eq $^tBu_3ArO^\bullet$ in DCM-d_2/1% MeCN-d_3 (v/v).

11. Select Reaction and Product Characterization of (2).

11.1. ^{1}H NMR of the completed reaction between 15.3 mM Tp^{tBuMe}Cu^{II}-OCH$_2$CF$_3$ and 1 eq TEMPO–H in DCM-d_2/1% MeCN-d_3 (v/v).

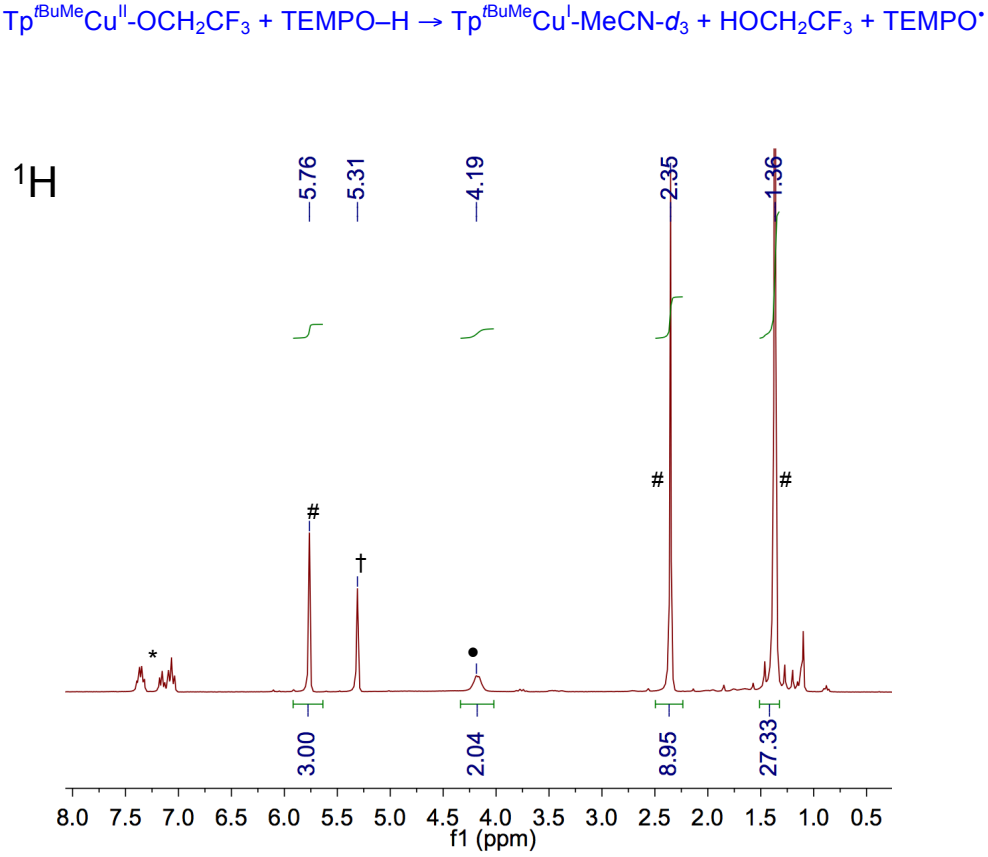

Figure S28. ^{1}H NMR spectrum of the completed reaction between 15.3 mM Tp^{tBuMe}Cu^{II}-OCH$_2$CF$_3$ and 1 eq TEMPO–H in DCM-d_2/1% MeCN-d_3 (v/v). Signals for Tp^{tBuMe}Cu^{I}–MeCN-d_3 are shown with #, TFE is shown with •, residual solvent signal with † and fluorobenzene internal standard with *.

11.2. ^{1}H NMR of the completed reaction between 15.3 mM Tp^{tBuMe}Cu^{II}-OCH$_2$CF$_3$ and 1 eq ^{t}Bu$_3$ArO–H in DCM-d_2/1% MeCN-d_3 (v/v).

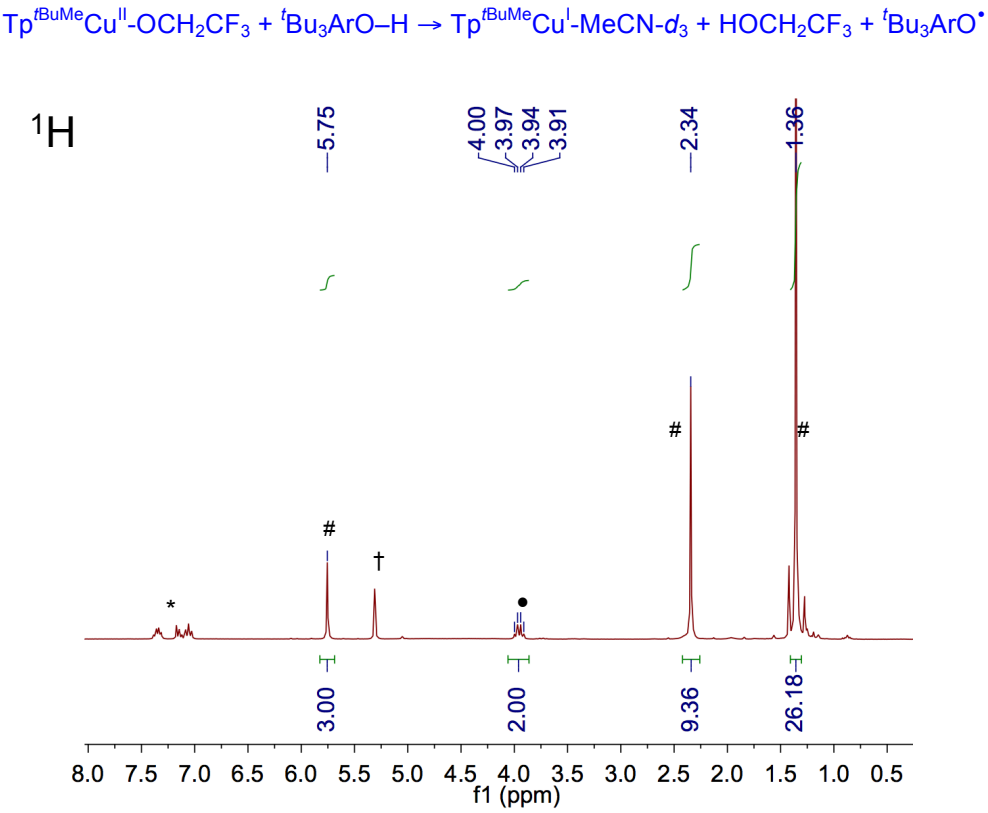

Figure S29. ^{1}H NMR spectrum of the completed reaction between 15.3 mM Tp^{tBuMe}Cu^{II}-OCH$_2$CF$_3$ and 1 eq ^{t}Bu$_3$ArO–H in DCM-d_2/1% MeCN-d_3 (v/v). Signals for Tp^{tBuMe}Cu^{I}–MeCN-d_3 are shown with #, TFE is shown with •, residual solvent signal with † and fluorobenzene internal standard with *.

11.3 ^{1}H NMR of the completed reaction between 15.3 mM Tp$^{t\text{BuMe}}$Cu^{II}-OCH$_2$CF$_3$ and 1 eq ABNO–H in toluene-d_8.

The reaction between Tp$^{t\text{BuMe}}$Cu^{II}-OCH$_2$CF$_3$ and ABNO–H was carried out in an NMR tube with 15.3 mM Tp$^{t\text{BuMe}}$Cu^{II}-OCH$_2$CF$_3$ and one equivalent of ABNO–H. After the reaction was complete (as determined by color change) the optical spectrum of the solution was collected. The resulting spectrum overlayed with an independently collected spectrum of 15.3 mM ABNO in toluene, indicating ABNO was generated quantitatively in this reaction.

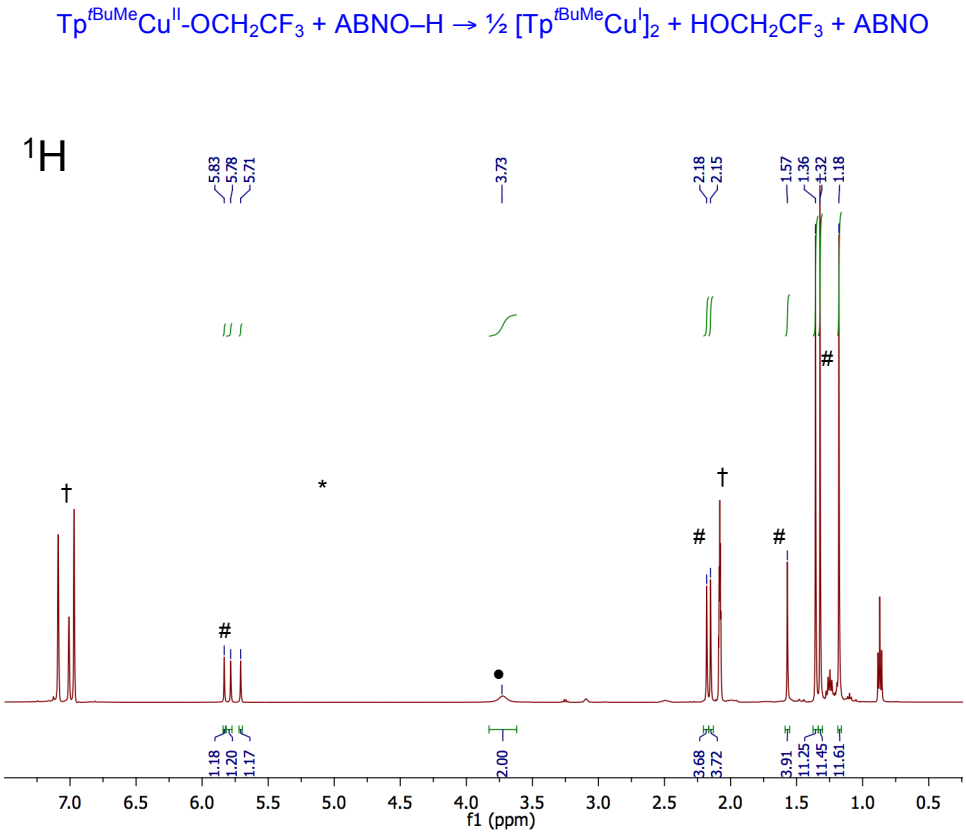

Figure S30 ^{1}H NMR spectrum of the completed reaction between 15.3 mM Tp$^{t\text{BuMe}}$Cu^{II}-OCH$_2$CF$_3$ and 1 eq ^{t}Bu$_3$ArO–H in toluene-d_8. Signals for [Tp$^{t\text{BuMe}}$Cu^{I}]$_2$ are shown by #, TFE is shown with • and residual solvent signal with †.

11.4 Kinetic Measurement Details for the Disproportionation Reaction of 15.3 mM $Tp^{tBu}Cu^{II}$-OCH_2CF_3 catalyzed with 1 eq TEMPO in DCM-d_2/1% MeCN-d_3 (v/v)

$$Tp^{tBuMe}Cu^{II}\text{-}OCH_2CF_3 + \text{TEMPO (catalytic; not consumed)} \rightarrow$$

$$Tp^{tBuMe}Cu^{I}\text{-MeCN-}d_3 + 0.5\ HOCH_2CF_3 + 0.25\ CF_3COOCH_2CF_3$$

Kinetics for this reaction were recorded in the same fashion as described above in 8.6, monitoring the appearance of the pyrazole-4-H signal integrated against a known concentration of fluorobenzene internal standard.

12. Select Reaction and Product Characterization of (3)

$Tp^{tBu}Cu^{II}$-$OCH(CH_3)CF_3$ displays similar reactivity to **(1)** and **(2)** in the experiments attempted but also undergoes a competing decomposition reaction.

11.1 Reaction of 15.3 mM $Tp^{tBu}Cu^{II}$-$OCH(CH_3)CF_3$ with 1 equivalent of TEMPO–H in DMC-d_2/1% MeCN-d_3 (v/v).

$$Tp^{tBu}Cu^{II}\text{-}OCH(CH_3)CF_3 + TEMPO\text{–}H \rightarrow Tp^{tBu}Cu^{I}\text{-}MeCN\text{-}d_3 + HOCH(CH_3)CF_3 + TEMPO^{\bullet}$$

This reaction occurs instantaneously and the products have been quantified by ^1H and ^{19}F NMR. The $HOCH(C\underline{H}_3)CF_3$ signal is covered by the ^{t}Bu signals from $Tp^{tBu}Cu^{I}$-MeCN-d_3.

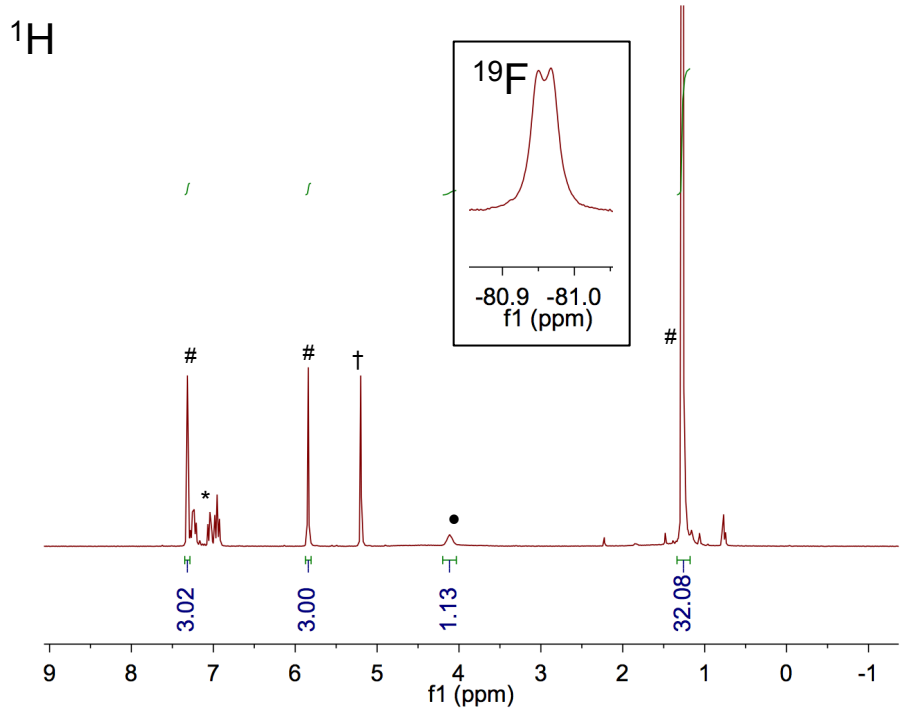

Figure S31. ^1H NMR spectrum of the completed reaction between 15.3 mM $Tp^{tBu}Cu^{II}$-$OCH(CH_3)CF_3$ and 1 equivalent of TEMPO–H showing the generation of $Tp^{tBu}Cu^{I}$-MeCN-d_3 and $HOCH(CH_3)CF_3$ (•). The residual solvent signal is shown by † and the fluorobenzene internal standard is shown by *. The inset displays the ^{19}F NMR signal for $HOCH(CH_3)CF_3$.

12.2. Reaction of 15.3 mM $Tp^{tBu}Cu^{II}$-$OCH(CH_3)CF_3$ with 1 equivalent of $^tBu_3ArO$–H in DMC-d_2/1% MeCN-d_3 (v/v).

$$Tp^{tBu}Cu^{II}\text{-}OCH(CH_3)CF_3 + {}^tBu_3ArO\text{–}H \rightarrow Tp^{tBu}Cu^{I}\text{-}MeCN\text{-}d_3 + HOCH(CH_3)CF_3 + {}^tBu_3ArO^{\bullet}$$

Reaction went to completion overnight. The products were confirmed by ^{1}H NMR with an internal standard and optically. The $HOCH(C\underline{H}_3)CF_3$ signal is covered by the ^{t}Bu signal of $Tp^{tBu}Cu^{I}$-MeCN-d_3.

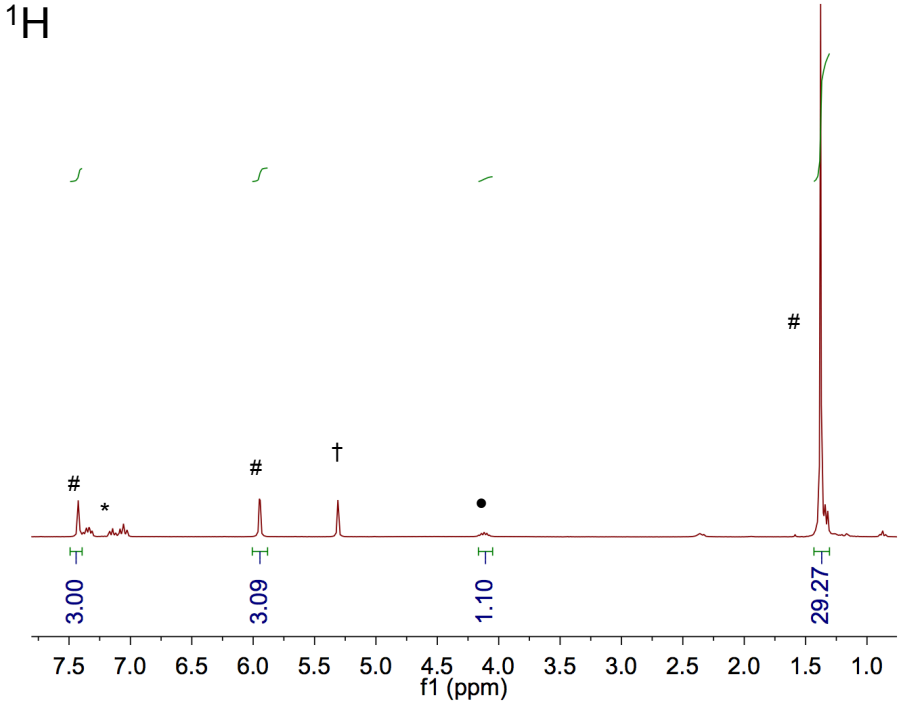

Figure S32. ^{1}H NMR spectrum of the completed reaction between 15.3 mM $Tp^{tBu}Cu^{II}$-$OCH(CH_3)CF_3$ and 1 equivalent of $^tBu_3ArO$–H showing the generation of $Tp^{tBu}Cu^{I}$-MeCN-d_3 and $HOCH(CH_3)CF_3$ (•). The residual solvent signal is shown by † and the fluorobenzene internal standard is shown by *.

12.3. ^{1}H and ^{19}F NMR Spectra of the Decomposition of Tp$^{t\text{Bu}}$Cu$^{\text{II}}$-OCH(CH$_3$)CF$_3$ in DCM-d_2/1% MeCN-d_3 (v/v).

$$Tp^{tBu}Cu^{II}\text{-}OCH(CH_3)CF_3 \rightarrow Tp^{tBu}Cu^{I}\text{-}MeCN\text{-}d_3 + 0.5\ HOCH(CH_3)CF_3 + ???$$

Decomposition of Tp$^{t\text{Bu}}$Cu$^{\text{II}}$-OCH(CH$_3$)CF$_3$ occurred overnight in either DCM-d_2/1% MeCN-d_3 (v/v) or toluene-d_8. When 1 equivalent TEMPO was added to Tp$^{t\text{Bu}}$Cu$^{\text{II}}$-OCH(CH$_3$)CF$_3$, the same decomposition products were observed but the reaction only required ~5 hours to reach completion. We were able to identify Tp$^{t\text{Bu}}$Cu$^{\text{I}}$-MeCN-d_3 and 0.5 equivalents of TFE as products but were unable to determine the identity of the other remaining product(s). Comparison of the ^{19}F NMR spectra of decomposition products of racemic or (*R*) enriched Tp$^{t\text{Bu}}$Cu$^{\text{II}}$-OC*H(CH$_3$)CF$_3$ indicates the unidentified product is diastereomeric (Fig S34).

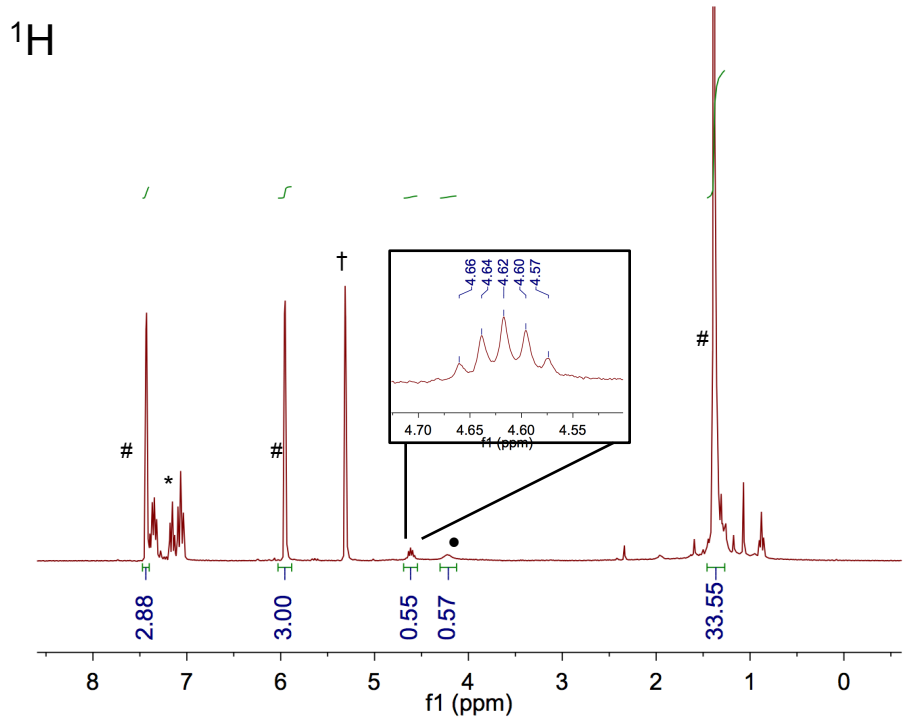

Figure S33. ^{1}H NMR spectrum (300 MHz) of the decomposition reaction of 15.3 mM Tp$^{t\text{Bu}}$Cu$^{\text{II}}$-OCH(CH$_3$)CF$_3$ in DCM-d_2/1% MeCN-d_3 (v/v). Tp$^{t\text{Bu}}$Cu$^{\text{I}}$-MeCN-d_3 is shown by #, trifluoroisopropanol by •, and residual solvent signal by †. The inset shows a close-up of the signal arising from the unknown product.

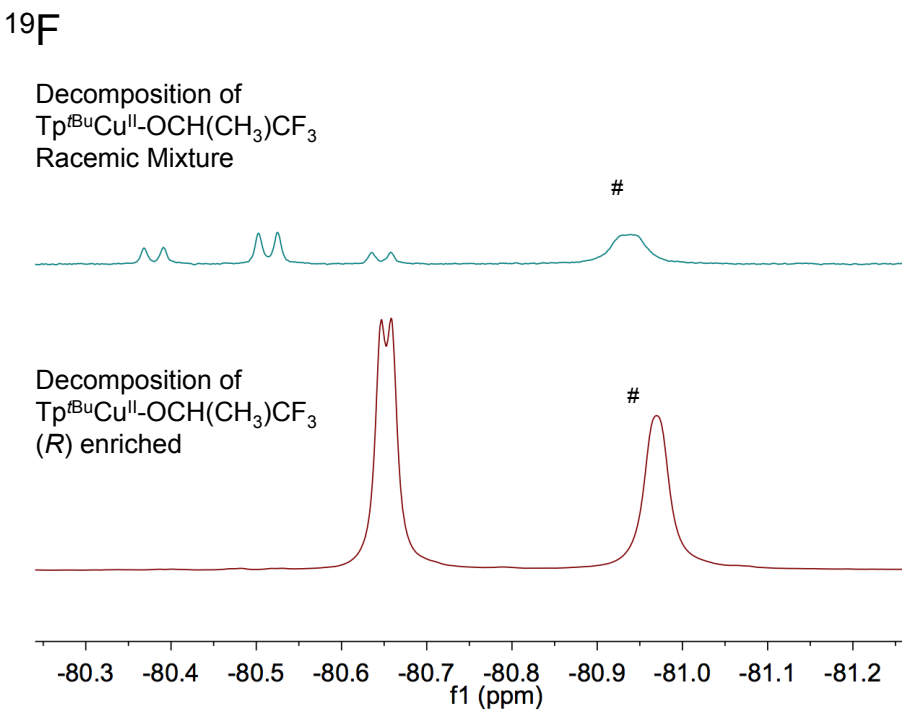

Figure S34. ^{19}F NMR spectra (282 MHz top; 470 MHz bottom) of the decomposition reaction of 15.3 mM or racemic $Tp^{tBu}Cu^{II}$-$OC^{*}H(CH_3)CF_3$ (top) or (*R*) enriched $Tp^{tBu}Cu^{II}$-$OC^{*}H(CH_3)CF_3$ (bottom) in DCM-d_2/1% MeCN-d_3 (v/v). Trifluoroisopropoxide is shown with #.

13. Thermochemical Analysis

13.1. Background

The interconversion between gas phase bond dissociation enthalpy (BDE) and bond dissociation free energy (BDFE) of X–H bonds can be achieved by using equation S1, using $S°(H^{\bullet}) = 27.42$ cal K^{-1} mol^{-1}.[8]

$$BDFE_g(X–H) = BDE_g(X–H) – TS°(H^{\bullet}) – T\{S°(X^{\bullet}) – S°(X–H)\} \quad (S1)$$

Typically for small molecules, $S°(X^{\bullet}) \cong S°(X–H)$ because they are generally very similar in size and structure. With this simplification, the relationship between $BDFE_g$ and BDE_g at 298K is simplified to equation S2.[8]

$$BDFE_g(X–H) = [BDE_g(X–H) – 8.2 \text{ kcal mol}^{-1}] \pm 0.5 \text{ kcal mol}^{-1} \quad (S2)$$

The interconversion between X–H gas phase BDFEs and solution BDFEs of can be achieved by accounting for the free energy of solvation of $H^{\bullet}$ and the difference in free energy of solvation of XH and $X^{\bullet}$ (equation S3).[8]

$$BDFE_{solv} = BDFE_g + \Delta G°_{solv}(H^{\bullet}) + [\Delta G°_{solv}(X^{\bullet}) – \Delta G°_{solv}(XH)] \quad (S3)$$

$\Delta G°_{solv}(H^{\bullet})$ in toluene is 4.77 kcal mol^{-1} (calculated from the solubility of $H^{\bullet}$ [assumed to be the same as H_2[6]] at STP (equation S4)).[8,9]

$$\Delta G°_{solv}(H^{\bullet}) = –RTln(K_{sol}) \quad (S4)$$

In aprotic solvents like toluene, the $[\Delta G°_{solv}(X^{\bullet}) – \Delta G°_{solv}(XH)]$ term is taken as the free energy of the XH–solvent hydrogen bond. This can be calculated using empirically determined H-bonding acidity (α_2^H) and basicity parameters (β_2^H) described by Abraham (equation S5).[10]

$$\Delta G°_{solv} = –10.02\alpha_2^H\beta_2^H – 1.492 \quad (S5)$$

The β_2^H parameter in toluene is 0.14.[11] Values for α_2^H have been extensively tabulated by Abraham.[12]

A more complete description of these conversions and the use of Abraham's model of interconverting solution BDFE values can be found in references 11.

13.2. Thermochemical Conversion Calculations

Calculating the BDFE of the first C–H bond of 1,4-cyclohexadiene in toluene:

The reported gas phase BDFE of the first C–H bond in 1,4-cyclohexadiene is 67.8 kcal mol^{-1}.[8]

The first C–H BDFE in toluene can be calculated using the reported gas phase BDFE of 67.8 kcal mol^{-1}. Using this value in equation S3 with the previously described $\Delta G°_{tol}(H^{\bullet}) = 4.77$ and assuming $\alpha_2^H \cong 0$,[8] the C–H $BDFE_{tol}$ is calculated to be 72.6 ± 3 kcal mol^{-1}.

Calculating the BDFE of the O–H bond of ABNO–H in toluene:

The gas phase BDE of ABNO–H is 76.2 kcal mol^{-1}.[10] This value is converted to a gas phase BDFE using equation S2: O–H $BDFE_g$ = 68 ± 2 kcal mol^{-1}.

Using this value in equation S3 with the previously described $\Delta G°_{tol}(H^{\bullet}) = 4.77$, toluene β_2^H = 0.14, and reported α_2^H = 0.39 for TEMPO–H (assumed to be the same for ABNO–H),[8] the $BDFE_{tol}$ value is calculated: O–H $BDFE_{tol}$ = 70.7 ± 3 kcal mol^{-1}.

Calculating the BDFE of the O–H bond in 2,2,2-trifluoroethanol, TFE, in toluene.

The gas phase BDE of CF_3CH_2O–H is 107.0 kcal mol^{-1}.[12] This value is converted to a gas phase BDFE using equation S2: O–H $BDFE_g$ = 98.8 ± 2 kcal mol^{-1}.

Using this value in equation S3 with the previously described $\Delta G°_{tol}(H^{\bullet}) = 4.77$, toluene β_2^H = 0.14, and reported α_2^H = 0.567 for TFE,[10] the $BDFE_{tol}$ value is calculated: O–H $BDFE_{tol}$ = 101.3 ± 3 kcal mol^{-1}.

Calculating the gas phase $\Delta G°_{dehydrog}$ of 2,2,2-trifluoroethanol.

The $\Delta H°_{g,dehydrog}$ can be calculated from the standard heats of formation of 2,2,2-trifluoroethanol (-211.3 kcal mol^{-1})[13] and trifluoroacetaldehyde (-185.8 kcal mol^{-1}; calculated).[13]

$CF_3CH_2OH \rightarrow 2C + 1.5\ F_2 + 0.5\ O_2 + 1.5\ H_2$	$\Delta H°_g = 211.3$ kcal mol^{-1}
$2C(s) + 1.5\ F_2 + 0.5\ O_2 + 0.5\ H_2 \rightarrow O=C(H)CF_3$	$\Delta H°_g = -185.8$ kcal mol^{-1}
$CF_3CH_2OH \rightarrow O=C(H)CF_3 + H_2$	$\Delta H°_{g,dehydrog} = 25.5$ kcal mol^{-1}

The enthalpy of dehydrogenation, $\Delta H°_{g,dehydrog}$, can be converted to a free energy of formation at 298K from the standard molar entropies of H_2 ($S°_g = 31.2$ cal mol^{-1} K^{-1}),[14] ethanol ($S°_g = 67.3$ cal mol^{-1} K^{-1})[14] and acetaldehyde ($S°_g = 63.0$ cal mol^{-1} K^{-1})[14] (taken to be the same as for 2,2,2-trifluoroethanol and trifluoroacetaldehyde).

$\{S°_g(H_2) + S°_g(\text{acetaldehyde})\} - S°_g(\text{ethanol}) = 26.9$ cal mol^{-1} K^{-1}

Thus, at 298 K, $\Delta G°_{g,dehydrog}$(2,2,2-trifluoroethanol) = 17.5 ± 3 kcal mol^{-1}

Other quoted BDFE values in toluene (taken to be the same as in benzene) are found in reference 8.

(8) Warren. J. J.; Tronic, T. A.; Mayer, J. M. *Chem. Rev.* **2010**, 110, 7062.
(9) Brunner, E. J. *J. Chem. Eng. Data*, **1985**, 30, 269.
(10) Abraham, M. H.; Grellier, P. L.; Prior, D. V.; Duce, P. P. *J. Chem. Soc. Perkin Trans. II*, **1989**, 699.
(11) Warren, J. J.; Mayer, J. M. *Proc. Natl. Acad. Sci.* **2010**, 107, 5282.
(12) Luo, Y. –R. *Comprehensive Handbook of Chemical Bond Energies*; CRC Press: Boca Raton, FL, 2007.
(13) Bartmess, J. E.; Liebman, *J. Struct. Chem.* **2013**, 24, 2035.
(14) *CRC Handbook of Chemistry and Physics*, 95th ed. CRC Press: Boca Raton, FL, 2014-2015.

14. Computational Details

The Gaussian 09 suite of programs was used for the calculation reported in this paper.[15] Geometry optimizations for $^{t}Bu_3$CHDO-TFE, $^{t}Bu_3$ArOH and trifluoroacetaldehyde were performed at M06/6-311+g(d,p) level[16] using density functional theory. Based on the results of geometry optimizations in the gas phase at the M06/6-311+G(d,p) level, all stable structures were fully re-optimized with the use of the PCM model of solvent (toluene) at the same level. Vibrational frequency calculations were carried out to confirm the stable structures for both gas-phase computation and SCRF computation.

(15) Frisch, M. J.; Trucks, G. W.; Schlegel, H. B.; Scuseria, G. E.; Robb, M. A.; Cheeseman, J. R.; Scalmani, G.; Barone, V.; Mennucci, B.; Petersson, G. A.; Nakatsuji, H.; Caricato, M.; Li, X.; Hrtchian, H. P.; Izmaylov, A. F.; Bloino, J.; Zheng, G.; Sonnenberg, J. L.; Hada, M.; Ehara, M.; Toyota, K.; Fukuda, R.; Hasegawa, J.; Ishida, M.; Nakajima, T.; Honda, Y.; Kitao, O.; Nakai, H.; Vreven, T.; Montgomery, J. A., Jr.; Peralta, J. E.; Ogliaro, F.; Bearpark, M.; Heyd, J. J.; Brothers, E.; Kudin, K. N.; Staroverov, V. N.; Kobayashi, R.; Normand, J.; Raghavachari, K.; Rendell, A.; Burant, J. C.; Iyengar, S. S.; Tomasi, J.; Cossi, M.; Rega, N.; Millam, J. M.; Klene, M.; Knox, J. E.; Corss, J. B.; Bakken, V.; Adomo, C.; Jaramillo, J.; Gomperts, R.; Stratmann, R. E.; Yazyev, O.; Austin, A. J.; Cammi, R.; Pomelli, C.; Ochterski, J. W.; Martin, R. L.; Morokuma, K.; Zakrzewski, V. G.; Voth, G. A.; Salvador, P.; Dannenberg, J. J.; Dapprich, S.; Daniels, A. D.; Farkas, O.; Foresman, J. B.; Ortiz, J. V.; Cioslowski, J.; Fox, D. J. GAUSSIAN 09, Revision A.01, Gaussian, Inc., Wallingford CT, 2009.

(16) (a) Zhao, Y.; Truhlar, D. G. *Acc. Chem. Res.* **2008**, 41, 157-167. (b) Valero, R.; Costa, R.; Moreira, I. P. R.; Truhlar, D. G.; IIIas, F. *J. Chem. Phys.* **2008**, 128, 114103.

Energetic parameters

Table S6. Calculated energetic parameters for $^{t}Bu_3$CHDO-TFE, $^{t}Bu_3$ArOH and trifluoroacetaldehyde at M06/6-311+G(d,p) level in the gas phase and in SCRF.

	trifluoroacetaldehyde	**$^{t}Bu_3$ArOH**	**$^{t}Bu_3$CHDO-TFE**
In the gas phase			
E	-451.462655	-778.367796	-1229.823177
H	-451.461711	-778.366852	-1229.822233
G	-451.497539	-778.437921	-1229.906142
SCRF			
E	-451.465090	-778.369966	-1229.826328
H	-451.464146	-778.369022	-1229.825384
G	-451.499992	-778.440253	-1229.908652

E: sum of electronic and thermal energies; ***H***: Sum of electronic and thermal enthalpies; ***G***: Sum of electronic and thermal free energies. All energies reported in units of Hartrees.

Cartesian Coordinates

Gas phase calculation

Trifluoroacetaldehyde

C	0.36168200	0.00826600	0.00002400
C	-1.06604000	-0.56113300	0.00010700
H	-1.08079400	-1.67185100	0.00023100
F	1.00676800	-0.43988900	-1.07877800
F	0.38509700	1.32301600	-0.00015500
F	1.00689100	-0.43960700	1.07881400
O	-2.03523200	0.12467200	0.00000600

$^{t}Bu_3ArOH$

C	-1.50590000	-0.37038500	-0.00015600
C	-0.53214000	-1.35597500	-0.00025000
C	0.83642300	-1.07329600	-0.00018800
C	1.21614100	0.27771600	-0.00011700
C	0.26641000	1.31838600	-0.00001400
C	-1.07266500	0.95353800	-0.00000400
H	-0.84317700	-2.39239300	-0.00033700
H	-1.82188800	1.73774200	0.00015100
O	2.52848600	0.66155500	-0.00004000
C	1.86794900	-2.21323900	0.00003000
C	2.73538800	-2.16812100	-1.26814500
C	2.73490100	-2.16773100	1.26851200
C	1.20331100	-3.59056500	0.00002100
H	2.10350700	-2.27455800	-2.15647400
H	3.30897600	-1.24575600	-1.40446900
H	3.45316500	-2.99679700	-1.26142800
H	2.10266400	-2.27398000	2.15660800
H	3.45268800	-2.99640000	1.26232300
H	3.30829300	-1.24522500	1.40464400
H	1.98057200	-4.36266500	0.00008500
H	0.58340100	-3.74786500	0.88882800
H	0.58348000	-3.74791100	-0.88882100
C	0.68299900	2.79378700	0.00001200
C	1.49631400	3.12005500	1.25858100
C	1.49627600	3.11993300	-1.25861500
C	-0.52741400	3.72664200	-0.00001200
H	0.90587200	2.91531700	2.15960600
H	2.41830300	2.54048400	1.31242100
H	1.75957000	4.18492000	1.26513400
H	0.90587700	2.91492300	-2.15960800
H	1.75939200	4.18483000	-1.26537800

H	2.41833500	2.54046500	-1.31232100
H	-0.17603400	4.76412600	0.00010000
H	-1.15244700	3.59220600	-0.89002600
H	-1.15258300	3.59205600	0.88988200
C	-3.00188700	-0.67394400	-0.00001100
C	-3.64809200	-0.07035400	1.25080800
C	-3.64883300	-0.06872700	-1.24965000
C	-3.29342200	-2.17156600	-0.00093800
H	-3.20541100	-0.49462600	2.15939700
H	-3.52250800	1.01618300	1.29500000
H	-4.72436300	-0.28190300	1.26482100
H	-3.20665400	-0.49171700	-2.15908000
H	-4.72509000	-0.28037900	-1.26331700
H	-3.52345400	1.01788300	-1.29248700
H	-4.37703100	-2.33420000	-0.00090800
H	-2.88691500	-2.66680400	-0.89026700
H	-2.88669800	-2.66798000	0.88762900
H	3.09772100	-0.10933900	-0.00056900

$^{t}Bu_3CHDO$-TFE

C	0.25105800	0.88002900	1.34659600
C	0.51960100	-1.42530200	0.52669900
C	1.58950100	-1.03311900	-0.17652900
C	1.77265600	0.39963500	-0.44859600
C	1.11116200	1.35823800	0.21673400
H	0.34329000	-2.47627800	0.72101500
H	2.48833100	0.67667800	-1.21828200
C	-1.35447900	-0.99946600	2.20155000
C	-0.46155300	-1.40723600	3.37330400
C	-2.39034200	0.02405900	2.67760600
C	-2.13260500	-2.22526800	1.71260400
H	0.25837100	-2.18542300	3.09519900
H	0.08994600	-0.55308000	3.77392400
H	-1.08496200	-1.81291700	4.17841500
H	-3.01950100	0.35978700	1.84764500
H	-3.04161600	-0.45022600	3.42071000
H	-1.92367700	0.89538100	3.13967600
H	-2.74151300	-2.60994300	2.53817000
H	-2.81965800	-1.96745600	0.89996500
H	-1.49203600	-3.05017700	1.38279100
C	2.60923500	-1.99269600	-0.76549300
C	2.34647300	-3.43873800	-0.36196700
C	2.54770500	-1.90457400	-2.29470800
C	4.00885700	-1.60578300	-0.27858400
H	2.37586200	-3.56796200	0.72583000

H	1.37769800	-3.79762100	-0.72798200
H	3.11848900	-4.08544500	-0.79272900
H	2.77982200	-0.90212600	-2.66839600
H	3.27278800	-2.59586600	-2.73945600
H	1.55048500	-2.17914600	-2.65970700
H	4.75517000	-2.28798700	-0.70172600
H	4.28697200	-0.58831800	-0.57145800
H	4.07147100	-1.66930300	0.81357900
C	1.25906200	2.84838400	-0.02814600
C	2.11037200	3.48838600	1.07515800
C	1.93010800	3.11900000	-1.37121200
C	-0.13169700	3.49124900	-0.05555400
H	1.64895300	3.37273000	2.05729800
H	3.10748000	3.03351600	1.10584200
H	2.23211300	4.55904400	0.87012300
H	1.38235200	2.65142000	-2.19825900
H	1.95164100	4.19883100	-1.55288800
H	2.96794200	2.76769400	-1.39635200
H	-0.03859200	4.56585600	-0.25003300
H	-0.74870000	3.05631000	-0.85059200
H	-0.65791800	3.36663800	0.89423700
C	-0.49083500	-0.43671900	1.04519500
O	0.15623600	1.49258900	2.38025300
O	-1.40988300	0.02775100	0.01360300
C	-1.38279200	-0.54455200	-1.25065900
H	-0.50902300	-0.23813900	-1.84973000
H	-1.41696200	-1.64384100	-1.23186100
C	-2.61494700	-0.07145500	-1.97991500
F	-2.63471900	1.25135100	-2.13488300
F	-3.73654000	-0.42285700	-1.35200900
F	-2.64152800	-0.62291500	-3.20092100

PCM model in SCRF

Trifluoroacetaldehyde

C	-0.36072300	0.00551900	-0.00003100
C	1.06653200	-0.56677700	-0.00010900
H	1.08526800	-1.67544400	-0.00028900
F	-1.00949900	-0.43674200	1.07857300
F	-0.37913100	1.32242100	0.00010300
F	-1.00967700	-0.43654100	-1.07854300
O	2.03308000	0.12509300	-0.00001000

$^{t}Bu_3ArOH$

C	-1.50488500	-0.37342500	-0.00010000
C	-0.52810800	-1.35664300	-0.00011400
C	0.84027100	-1.07151500	-0.00005300
C	1.21662900	0.28088800	-0.00002100
C	0.26378500	1.31942800	0.00000300
C	-1.07507900	0.95187000	-0.00001800
H	-0.83651700	-2.39387300	-0.00016300
H	-1.82623200	1.73426200	0.00003600
O	2.52754000	0.66855100	0.00003200
C	1.87341100	-2.21030100	-0.00000600
C	2.74059800	-2.16380100	-1.26820000
C	2.74064000	-2.16365100	1.26815800
C	1.20942000	-3.58797600	0.00008700
H	2.10903800	-2.26862800	-2.15700500
H	3.31759700	-1.24328100	-1.40175700
H	3.45648100	-2.99389700	-1.26146600
H	2.10910700	-2.26840500	2.15699100
H	3.45653600	-2.99373500	1.26148400
H	3.31760700	-1.24309700	1.40158100
H	1.98795000	-4.35856200	0.00015000
H	0.59002800	-3.74596300	0.88916600
H	0.59004500	-3.74609700	-0.88898100
C	0.67594500	2.79635400	0.00005000
C	1.48830100	3.12525800	1.25863100
C	1.48826000	3.12533800	-1.25853600
C	-0.53690900	3.72616800	0.00009600
H	0.89708600	2.92166600	2.15949400
H	2.41057600	2.54604700	1.31402100
H	1.75045300	4.19042900	1.26358800
H	0.89700700	2.92182700	-2.15939200
H	1.75043400	4.19050400	-1.26342000
H	2.41052100	2.54611100	-1.31400000
H	-0.18765300	4.76441900	0.00014400
H	-1.16178600	3.58979300	-0.88966700
H	-1.16178400	3.58970800	0.88984800
C	-3.00016800	-0.68134700	-0.00004700
C	-3.64854400	-0.07896300	1.25033900
C	-3.64893500	-0.07800700	-1.24976900
C	-3.28730200	-2.17984700	-0.00060100
H	-3.20607400	-0.50289800	2.15930600
H	-3.52583900	1.00798800	1.29426400
H	-4.72418500	-0.29358100	1.26282200
H	-3.20670600	-0.50118500	-2.15920500
H	-4.72456000	-0.29270300	-1.26209700
H	-3.52636100	1.00898900	-1.29288400

H	-4.37056600	-2.34472100	-0.00063100
H	-2.87919200	-2.67418800	-0.88967000
H	-2.87915200	-2.67487600	0.88806400
H	3.10184000	-0.09943800	-0.00026400

$^{t}Bu_3CHDO$-TFE

C	0.14423900	0.80704400	1.40515500
C	0.58998200	-1.44068000	0.46973100
C	1.64987900	-0.94452300	-0.18095300
C	1.75794100	0.51051900	-0.35141400
C	1.01825700	1.39116900	0.34010400
H	0.46474500	-2.51045700	0.58336900
H	2.48222900	0.87493400	-1.07456200
C	-1.33244500	-1.23429400	2.12565400
C	-0.44841600	-1.59514200	3.31854300
C	-2.48867200	-0.34413200	2.58858800
C	-1.95944500	-2.51374400	1.56130800
H	0.38991700	-2.23986600	3.02990100
H	-0.04622800	-0.70339000	3.80528400
H	-1.04374900	-2.14352200	4.05766200
H	-3.14991000	-0.09378300	1.75364600
H	-3.07935600	-0.89227200	3.33163900
H	-2.13991200	0.58041400	3.04864900
H	-2.63275300	-2.94034700	2.31281400
H	-2.55991700	-2.30546000	0.66915200
H	-1.22580500	-3.28879800	1.31865200
C	2.72153900	-1.80553400	-0.82786600
C	2.54183000	-3.28585900	-0.51453900
C	2.64354500	-1.62602800	-2.34917800
C	4.10050200	-1.37050200	-0.32361400
H	2.57442900	-3.47758700	0.56390700
H	1.59653400	-3.67659000	-0.90783200
H	3.35141400	-3.85817300	-0.97970400
H	2.81316900	-0.59058800	-2.66187000
H	3.40557400	-2.24422300	-2.83763400
H	1.66206100	-1.93741900	-2.72697000
H	4.87925100	-1.98484600	-0.78972300
H	4.32124200	-0.32447600	-0.55859000
H	4.17445500	-1.49475500	0.76263900
C	1.07810600	2.89773000	0.16465600
C	1.80409600	3.55345100	1.34552700
C	1.81769600	3.27242800	-1.11617800
C	-0.35196000	3.43963300	0.06076000
H	1.28549600	3.37381800	2.28903200
H	2.82592000	3.16562500	1.43263400

H	1.86577400	4.63613300	1.18117600
H	1.35613000	2.81447400	-1.99957800
H	1.78380400	4.35926300	-1.24699800
H	2.87412200	2.98237000	-1.08497900
H	-0.32614800	4.52364000	-0.09901000
H	-0.88299700	2.98557800	-0.78503700
H	-0.92909700	3.24805900	0.96910800
C	-0.48624600	-0.54761500	1.02340000
O	-0.05723800	1.37613500	2.45015100
O	-1.42828500	-0.09560600	0.00398800
C	-1.28035200	-0.49416200	-1.31786700
H	-0.41375100	-0.03209500	-1.82037700
H	-1.20917400	-1.58533600	-1.43820100
C	-2.51796200	-0.03797100	-2.04618800
F	-2.66500200	1.28733000	-2.01385100
F	-3.62807200	-0.57885700	-1.54075700
F	-2.43981200	-0.40350300	-3.33262300